Co-simulation of ship motions and sloshing in tanks

Gabriele Bulian [a,*], Jose Luis Cercos-Pita [b,c]

[a] Department of Engineering and Architecture, University of Trieste, Via A. Valerio 10, 34127 Trieste, Italy
[b] CEHINAV Research Group, ETSIN, Technical University of Madrid (UPM), 28040 Madrid, Spain
[c] ETSIAE, Technical University of Madrid (UPM), 28040 Madrid, Spain

ARTICLE INFO

Keywords:
6-DOF nonlinear blended seakeeping
Smoothed-particle hydrodynamics (SPH)
Sloshing
Co-simulation
Anti-rolling tanks (ART)
Validation

ABSTRACT

Ship dynamics in presence of sloshing is addressed in time-domain through a co-simulation approach. A nonlinear blended 6-DOF ship motion solver, addressing rigid body dynamics and external fluid-structure interaction, is coupled with a 3D Weakly Compressible Smoothed-Particle Hydrodynamics (WC-SPH) solver, addressing the internal fluid dynamics. The coupling is carried out by means of network communication, which is suitable for grid computing. The resulting co-simulation approach is able to address nonlinear ship motions together with nonlinear sloshing in internal tanks. The two solvers and the co-simulation strategy are presented, together with two example applications. One example application addresses the roll motion of a vessel, with and without an anti-rolling tank, in regular beam waves. The effect of varying the anti-rolling tank length and the effect of varying the forcing wave steepness are investigated. Simulations disclose nonlinear phenomena and indicate the capability of the developed approach of identifying the reduction of anti-rolling tank effectiveness for too small tank lengths and/or too large forcing wave steepnesses. A second application is presented, for validation purposes, where simulations are compared with experimental data from literature regarding roll and heave for a tanker hull form in regular beam waves, with and without a partially filled tank.

1. Introduction

The normal operating conditions of vessels are almost invariably characterised by the presence of liquids onboard, which are contained in appropriate tanks. Fuel, fresh water and ballast water represent the most common liquids carried by basically all cargo and passenger vessels in certain loading conditions. In addition, there are types of vessels, such as tankers, LNG carriers, etc., carrying a large quantity of liquids as cargo, i.e. the payload of the ship. Liquids represent also the payload of FPSOs, where the cargo is stored before being offloaded. There are also cases (e.g. fishing vessels, offshore supply vessels) where partially filled tanks can be fitted onboard with the scope of acting as anti-rolling devices. Anti-rolling tanks (ART) could be considered to represent for ships what tuned liquid dampers (TLD) represent for buildings (Bulian et al., 2010). Indeed, in both cases, a secondary system (the ART or the TLD) is attached to, and forced by, the primary system (the vessel or the building), and the force generated by the secondary system on the primary system is meant to counteract the external forcing on the primary system (waves, wind, earthquake), with the final scope of reducing the motion of the primary system.

The exact calculation of reduction of ship restoring capabilities due to the presence of partially filled tanks in purely quasi-static conditions (the so-called "free surface effect") is, nowadays, a matter of routine static stability calculations for ships and offshore floating structures. On the other hand, the same cannot be said when ship dynamics and fluid cargo dynamics are to be accounted for in a fully (two-way), or even partially (one-way), coupled way. Due to the complexity of the involved phenomena, a coupled dynamic approach is particularly challenging, especially when nonlinear effects are to be considered in both ship motions and flow inside the tank.

1.1. Background

In view of the modelling complexity involved in the problem of coupled ship motions and sloshing in partially filled tanks, a variety of different approaches have been developed in the past in order to address it at different levels of sophistication. Broadly speaking, the various approaches can be categorised depending on the type of modelling used for ship motions (linear vs nonlinear) and for the fluid within the tank (linear vs nonlinear). However, intermediate approaches can also be found where only limited nonlinearities are introduced. Typically, fully linear approaches allow exact frequency domain solution. In some cases, when

* Corresponding author.
E-mail addresses: gbulian@units.it (G. Bulian), jl.cercos@upm.es (J.L. Cercos-Pita).

Accepted 5 January 2018

nonlinearities are introduced, e.g. on roll damping and/or roll restoring, approximate solutions for the response of the dynamical system could be obtained, in principle, by means of linearization techniques, which, in case of stochastic excitation or deterministic excitation, basically allow addressing the problem in frequency domain (e.g. Francescutto and Contento, 1999b; Hayashi, 1964; Roberts and Spanos, 2003). However, in the more general cases, the introduction of significant nonlinearities requires moving from frequency domain approaches to time domain approaches, since approximate techniques can no longer be used due to reduction in accuracy and/or complexity of application, or simply because of impossibility of application. It is also noted that there can be advantages in using time domain approaches, instead of frequency domain ones, also for the simulation of linear ship motions in waves in presence of forward speed, as proposed and discussed by Colagrossi et al. (2001).

In the following, an introductory literature survey is reported, focussing in particular, on studies addressing ship motions in presence of fluids onboard. Reviewed approaches are separated into those based on linear modelling of ship motions, and those based on nonlinear modelling of ship motions.

1.1.1. *Approaches based on linear ship motion models*

Fully linear potential approaches for ship motions, internal and external hydrodynamics have been developed by Malenica et al. (2003) and Kim and Shin (2008). In such approaches both ship motions and fluid in onboard tanks are treated in the framework of linear inviscid potential theory. As a result, the problem can be formulated and solved in frequency domain. Such approaches are very suitable for design purposes in mild sea conditions because they are computationally fast and they allow having a wide picture of the coupled dynamics. Furthermore, another positive characteristic of fully linear approaches is that the modelling is theoretically consistent. At the same time, however, linear approaches suffer from a series of limitations. Dissipation effects from the fluid within the tank are not accounted for by the potential framework, and this requires the introduction of artificial damping in the tank (Kim and Shin, 2008; Malenica et al., 2003) which usually implies some tuning (Moirod et al., 2010). Similarly, viscous damping effects need to be introduced for ship motions with reference to the external fluid-structure interaction problem, particularly for roll. In addition, by their very essence, linear approaches completely miss all those phenomena related to sloshing and/or to ship motions which are specifically driven by nonlinearities and/or time dependent parameters (for instance: parametric roll, parametrically excited sloshing, bending of roll or of sloshing response curves, sub-harmonic and ultra-harmonic resonances, violent sloshing flows with multi-valued free surface elevation and/or fragmentation, etc.).

In those situations where ship motions can be considered small, but nonlinearities need to be considered for the fluid motions inside the tank, a mixed approach can be used. In such a mixed approach, a linear model addressing rigid body dynamics and external fluid-structure interaction is coupled with a more sophisticated modelling of the internal flow dynamics. In such a framework, simulations are typically carried out in time domain. This type of approach was followed, for instance, by Kim et al. (2007), where a time domain linear model for rigid body ship dynamics and external fluid-structure interaction was coupled with a finite-difference solution of Navier-Stokes equations for the fluid in the tank, assuming that the free surface is single valued. A similar approach was also followed by Zhao et al. (2014), where a linear time domain ship motions model was coupled with the solution of the internal sloshing problem modelled as a nonlinear potential flow with artificial dissipation added to the dynamic boundary condition on the free surface. The possibility of handling complex, non-single valued, free surface dynamics was instead considered by Bunnik and Veldman (2010), where a volume of fluid (VOF) solver for the internal sloshing flow was coupled in time domain with a linear ship motions model. More recently, a time domain coupling has been presented by Serván-Camas et al. (2016) between a linear FEM solver for external fluid-structure interaction, and the nonlinear SPH solver AQUAgpusph used also herein, considering linear rigid body dynamics. Dillingham (1981) coupled a time domain ship motions model based on linear ship dynamics and quadratic nonlinearities in roll and sway damping, with a nonlinear shallow water solver for simulating ship motions coupled with water on deck, considering also inflow/outflow from scuppers. It is worth noting, however, that mixing a linear model for rigid body motions with a nonlinear model for the flow inside the tank can easily lead to modelling inconsistencies. A typical example of inconsistent coupling is associated with the proper handling of the kinematics when the boundary conditions for the nonlinear fluid solver are expected to be provided accounting for fully nonlinear rigid body motions. In fact, when motions are available only in a linear framework, the exact nonlinear rigid body kinematics is lost in the linearization process and it cannot be exactly recovered. As a consequence, in such situation, linear kinematics cannot provide exact nonlinear boundary conditions for the fluid dynamics solver.

1.1.2. *Approaches based on nonlinear ship motion models*

However, there are several situations where ship motions cannot be considered small enough to justify the linearization of rigid body ship dynamics and of the external fluid-structure interaction problem. In general, this is the case when the interest is on the assessment of ship behaviour in severe environmental conditions, or when there is specific interest on typically nonlinear dynamic stability phenomena in waves, such as, for instance, those identified as potentially dangerous by the International Maritime Organization (IMO, 2009): parametric roll, pure loss of stability, surf-riding and broaching, large amplitude roll in dead-ship condition. Similarly, ship motions cannot be addressed through a linear approach whenever the interest is on the simulation of the behaviour of a vessel which is free running in wind and waves (e.g. Bulian et al., 2015; de Kat and Paulling, 1989; Matusiak, 2007). In all such cases, it is necessary to describe the dynamics of the vessel by means of nonlinear models. In this respect, the case of roll motion is particularly relevant. In fact, roll motion very often needs to be addressed through nonlinear approaches both for damping (as a minimum) and for restoring, even in conditions where the other relevant motions (e.g. heave and pitch) can be treated linearly without significant loss of accuracy.

Coupled ship motions and sloshing models, accounting for nonlinearities in ship dynamics, and in particular in roll, have been developed, in several cases, by using simplified nonlinear models with a reduced number of degrees of freedom (DOF). Francescutto and Contento (1999a) coupled a 1-DOF nonlinear model for roll in regular beam waves, with the linear mechanical equivalent system developed by Graham and Rodriguez (1952) for a rectangular tank partially filled with liquid. A pendulum-like (lumped mass) mechanical model was instead used by Spanos and Papanikolaou (2001) to mimic the sloshing behaviour of water trapped on deck of a fishing vessel. The lumped mass approach was also used in case of damaged ship condition for mimicking the sloshing behaviour in flooded compartments by Papanikolaou et al. (2000) and, later, by, e.g., Jasionowski (2001), Fujiwara and Haraguchi (2005), Manderbacka et al. (2015). For tanks in forced motion, results from application of the lumped-mass approach have been compared with simulations based on Moving Particle Semi-Implict (MPS) by Fonfach et al. (2016), and with VOF, through OpenFOAM, by Manderbacka et al. (2014), making reference, in both cases, also to experimental reference tests. Taguchi et al. (2003) coupled a nonlinear 1-DOF roll model with a linear 1-DOF model of U-tube anti-rolling tank, and performed numerical bifurcation analyses with the intention of investigating nonlinear motions starting from observations from experimental tests for a fishing vessel in condition of reduced initial stability. The fully linearized version of the modelling used by Taguchi et al. (2003) was also used by Tanizawa et al. (2003), and results were compared with experiments and with simulations from a fully nonlinear two-dimensional time domain BEM potential approach for external (ship-waves) as well as internal

(ship-tank) fluid structure interaction where viscous effects were accounted for by means of artificial additional dissipation terms. Neves et al. (2009) coupled a simplified 3-DOF dynamical model of heave, roll and pitch with a simplified 1-DOF model of a U-tube (passive/active) anti-rolling tank. The scope of the analysis was to address the effect of the tank on the limits of inception (instability regions) and on the magnitude (when excited) of parametric roll in regular longitudinal waves. A more sophisticated approach was instead used by Hashimoto et al. (2012) with the aim of taking into account the exact nonlinear flow behaviour within the tank. To this end, Hashimoto et al. (2012) coupled a 1-DOF nonlinear roll motion model for parametric roll in regular head waves with a Moving Particle Semi-implicit (MPS) solver for the internal flow. In order to take into account, at least approximately for design purposes, nonlinearities of the fluid flow in free-surface tanks, Carette (2015) has proposed a methodology based on the use of motion amplitude dependent retardation functions for modelling the action of fluid in forced tanks. Carette (2016) later used such approach by coupling it with a 1-DOF roll motion model and with the 6-DOF blended code FREDYN used in 3-DOF mode considering roll, sway (softly restrained) and heave. Computed roll responses and distributions of roll peaks were compared with experimental results in irregular waves.

However, in order to fully describe ship dynamics in the general cases, it is necessary to use models considering the whole set of 6-DOF, taking into account nonlinearities, with reference, at least, to those associated with rigid body kinematics and to those which are most relevant for the problem under consideration. Moreover, non-zero forward speed is also to be taken into account. Modelling along this line have been used, for instance, by Holden and Fossen (2012) and by Mitra et al. (2012). The former considered a 6-DOF dynamical ship motions model coupled with a 1-DOF model for a passive U-tube tank, while the latter used a similar ship motions model, but addressed the sloshing in the tank through a FEM solution of the internal flow in the framework of the nonlinear potential flow modelling. Huang and Hsiung (1996) coupled a time domain hybrid 6-DOF ship motions model with a numerical flow solver based on shallow water equations, and simulated the behaviour of fishing vessels in waves with and without the presence of a constant amount of water on deck. The shallow water approximation was also used by Greco and Lugni (2012), Liut et al. (2013) and Greco et al. (2014) for simulating nonlinear ship motions in presence of water on deck.

1.2. Objectives

The analysis of the available literature clearly indicates that approaches presented in the past for the simulation of ship motions in presence of free surface tanks are numerous and diversified. However, there seems to be space for improvements regarding simulation approaches which can be able to address significant nonlinear effects, both in ship motions and in the internal flow behaviour, considering 6-DOF for the vessel. The aim of this study is, therefore, to contribute in this respect by presenting a simulation approach fulfilling a series of requirements:

- It must be able to take into account nonlinear 6-DOF motions of a vessel, which, potentially, is self-propelled and manoeuvring in realistic wind and waves;
- It must be based on a full two-way coupling with internal tanks containing fluid;
- It must be able to simulate three dimensional nonlinear sloshing, possibly characterised by violent impacts, wave breaking and plunging, free surface fragmentation, etc., taking into account the fluid viscosity, without specific restrictions on the actual filling level of the tank;
- It must be able to consider generic tanks' shapes;
- It must be fast enough for practical applications.

The above objectives are set in such a way that the simulation approach can address, with a reduced number of approximations, the actual behaviour of a vessel at sea in presence of tanks carrying liquids. In addition to the general scientific interest, such an approach can be of practical relevance for the already mentioned example cases of tankers, LNG carriers, FPSOs, vessels fitted with anti-rolling tanks.

In order to try achieving the reported set of objectives, this paper, by building on and significantly extending a previous short paper (Cercos-Pita et al., 2016), describes a simulation approach where a blended 6-DOF nonlinear ship motion code is coupled with a fully nonlinear Smoothed-Particle-Hydrodynamics (SPH) solver for the solution of the fluid dynamics in the tank. The reasons behind the choice of these tools are clarified at the beginning of the next section. Afterwards, the main modelling characteristics of the two tools are described, followed by a description of the coupling strategy which is based on communication carried out through Transmission Control Protocol/Internet Protocol (TCP/IP). In the subsequent section an example application is presented. In the example application, a vessel (based on a freely available hull geometry) is equipped with a free surface tank intended to act as an anti-rolling tank (ART), and a set of experiments without tank are used to tune the ship motions code. The effect of different ART lengths and the effect of different forcing wave steepnesses are investigated in regular beam waves. For validation purposes of the coupled code, a separate appendix presents comparisons between experiments and simulations for another case available from de Kat (2000). Simulation performance are also discussed. Finally, a series of conclusions are reported, together with needs for future work.

2. Simulation tool

A simulation tool fulfilling the target requirements described in the previous section shall be able to address general, and possibly significantly nonlinear, motions of a ship with liquid tanks onboard in realistic environment. Since nonlinearities are to be taken into account, a fully linear coupled approach (e.g. Kim and Shin, 2008; Malenica et al., 2003) is unfortunately not a viable option, even if supplemented by some weak nonlinearities (such as, e.g., nonlinear ship roll damping). On the completely opposite side of the spectrum of modelling sophistication, there would be fully coupled simulation approaches based on direct viscous CFD computations for both the external fluid-structure interaction, as well as for the solution of the internal flow. The available literature indicates that research is ongoing on direct CFD simulation of nonlinear ship motions and/or free running ships in waves (e.g. Carrica et al., 2012; Kawamura et al., 2015; Sadat-Hosseini et al., 2010, 2011). Examples are also available in literature regarding simulation of ship motions in waves for vessels with partially filled tanks, taking into account both the external and the internal fluid-structure interaction through direct viscous CFD approaches (e.g. Peric et al., 2009). However, the required computational time and resources are still prohibitively large for practical systematic applications, particularly for those cases where large computational domains and long simulations are considered.

Considering the above, an intermediate approach has therefore been followed herein, trying to balance simplicity, accuracy and computational time. The idea is to use, and couple, two different simulation tools. One tool is intended, and specialized, for dealing with the internal flow. The second tool is instead intended, and specialized, for dealing with ship motions and external flow. A benefit of addressing the two problems using different simulation strategies is the possibility of using simulation paradigms which, separately, have been proved to be suitable for the intended use, and which can therefore be assumed to be suitable for the intended use also when coupled together. This also facilitates, in principle, the verification and validation process, as well as the tuning process (when necessary), since these processes can be carried out separately for each tool. An approach conceptually similar to the one selected for the present study was used by Gao et al. (2013) for the case of a damaged vessel.

For the simulation of 6-DOF ship dynamics, a reduced complexity

approach has been selected, based on so-called "blended" (or "hybrid") tools. Such tools, following the line initiated by de Kat and Paulling (1989), comprise several sub-models handling different physical aspects of the problem. The combination of all the sub-models is intended to handle, in an approximate way, the external fluid-structure interaction problem, as well as the propulsion and steering (when relevant). Models for mooring lines, or simplified linear/nonlinear springs, can also typically be introduced, when necessary. The main scope of blended tools is to try addressing what are considered to be the most relevant effects in the fluid-structure interaction, in conditions possibly characterised by large amplitude nonlinear motions and/or manoeuvring in wind and waves. At the same time, such tools are designed with the fundamental requirement of keeping the computational efforts at an acceptable level for practical applications. Experience has shown that blended tools can provide good motions predictions for practical applications. Such tools have also been recently considered to be suitable for the so-called "direct intact stability assessment" in the framework of the development of International Maritime Organization (IMO) "Second Generation Intact Stability Criteria" (see, e.g. Bulian and Francescutto, 2013; Bulian et al., 2015; Peters et al., 2011; and references therein). The main drawback of such tools is that, being them characterised by a significant level of model reduction, they require tuning of the sub-models' coefficients. The extent to which this tuning is required typically depends on the specific application. Furthermore, a proper tuning requires a good understanding of the underlying limitations and interrelation of various sub-models. Globally, considering pros and cons, a blended approach has been considered to represent a suitable balance of simplicity, accuracy and computational time, for the intended use in this study. Recent developments regarding blended ship motions simulation approaches have been discussed by Bačkalov et al. (2016).

With reference to the internal flow dynamics, the requirement of being able to address violent flows with possibly non-single-valued free surface, in arbitrary shaped, and sometimes complex, tank geometries, limit the choices in terms of possible simulation approaches. Some existing approaches for the internal flow simulation, which are fulfilling the former requirements, have already been used in the past: VOF (Bunnik and Veldman, 2010), FEM (Mitra et al., 2012), and MPS (Hashimoto et al., 2012). In making reference to different simulation approaches, it is also worth recalling that the equivalence between MPS and incompressible SPH (I-SPH) has been proved by Souto-Iglesias et al. (2013, 2014). All these approaches are truly incompressible formulations, i.e. they are requiring the solution of the Poisson equation for the pressure at each time step. Unfortunately, the solution of the Poisson equation requires a computational effort which can be too high for practical applications, which are instead targeted in the context of this study.

To avoid solving the linear system coming from the Poisson equation, the weakly compressible SPH (WC-SPH) methodology can be applied. Although the resulting fluid is not truly incompressible, the density variations are very small and thus negligible for practical purposes. In principle, due to the large number of interactions per particle, and the required small time steps, WC-SPH can be as much computational expensive as VOF or FEM. However, Hérault et al. (2010), Crespo et al. (2011) and Domínguez et al. (2013) demonstrated that very large speed-ups can be achieved by using Graphics Processing Units (GPU) based devices. On the other hand, it seems that the performance of VOF, FEM and MPS solvers cannot be improved to the same extent by using GPUs (Göhner, 2010). For such reasons, it has been decided to use a simulation method for the internal flow based on weakly-compressible-SPH (WC-SPH) (see Monaghan, 2005; Colagrossi et al., 2009; and references therein).

In order to setup the global simulation framework, in addition to the underlying simulation tools, it is also necessary to specify a strategy for making the tools collaborating. Such strategy strongly depends on how the two tools are planned to interact. In some cases, the two tools can be recoded in such a way to embedded them into a single simulation code. However, this is not always possible, especially when the two tools run, or are intended to run, on different hardware architectures. In such case, which is actually the case dealt with in this work, a co-simulation strategy should be used. A co-simulation strategy of the type used herein has been used in the past in the automotive context by Elliott et al. (2006) and Fleissner et al. (2010), while other examples relevant to the present study have been presented by Breuer et al. (2012) and Gomes et al. (2011).

In the following, the main characteristics of the 6-DOF blended ship motions simulations model, of the WC-SPH simulation model for the internal flow, and of the co-simulation strategy are described.

2.1. Rigid body ship dynamics and external fluid-structure interaction

The blended 6-DOF ship motion simulation code used in this study is called SHIXDOF ("nonlinear SHIp motion simulation program with siX Degrees Of Freedom") (Bulian and Francescutto, 2013; Bulian et al., 2012, 2015). The simulation strategy used in SHIXDOF is of the "blended" type because different sub-models, coming from different fields of ship motions, manoeuvring and propulsion are, indeed, blended together with the intention of solving the ship nonlinear rigid body dynamics in wind and waves. The resulting simulation approach is therefore a system-based simulation method.

Ship dynamics is dealt with by using two reference systems: a ship fixed reference system $S : Oxyz$, and an earth-fixed reference system $\Sigma : \Omega\xi\eta\zeta$. The ship-fixed reference system $S : Oxyz$ is used to project rigid body dynamics equations (as it is common in manoeuvring simulations). The earth-fixed reference system $\Sigma : \Omega\xi\eta\zeta$ is the reference system with respect to which the ship is actually positioned and oriented. In addition, $\Sigma : \Omega\xi\eta\zeta$ is used for the specification of wave elevation and wave-related fields (velocity and pressure) and, if necessary, of the wind speed field.

Rigid body dynamics equations, projected in the ship fixed reference system $S : Oxyz$, take the following vector form:

$$\begin{cases} m\left[\underline{u}_O^{'} + \underline{\omega} \wedge \underline{u}_O + \underline{\omega}^{'} \wedge \underline{x}_G + \underline{\omega} \wedge (\underline{\omega} \wedge \underline{x}_G)\right] = \underline{F}_{ext}(t) \\ \underline{\underline{I}}_O \underline{\omega}^{'} + \underline{\omega} \wedge (\underline{\underline{I}}_O \underline{\omega}) + m\underline{x}_G \wedge \underline{u}_O^{'} + m\underline{x}_G \wedge (\underline{\omega} \wedge \underline{u}_O) = \underline{M}_{ext,O}(t) \end{cases} \tag{1}$$

In (1), single underlining indicates vectors, double underlining indicates matrices. Furthermore, m [kg] is the ship mass, $\underline{u}_O = (u, v, w)^T$ [m/s] is the speed vector of the centre of the ship-fixed reference system (which does not coincide, in general, with the centre of gravity of the ship), $\underline{\omega} = (p, q, r)^T$ [rad/s] is the rigid body angular velocity, $\underline{x}_G = (x_G, y_G, z_G)^T$ [m] is the position vector of the centre of gravity in the ship-fixed reference system, $\underline{\underline{I}}_O$ [kg·m^2] is the tensor of inertia with respect to the centre O of the ship-fixed reference system, $\underline{F}_{ext}(t) = (F_{ext,x}(t), F_{ext,y}(t), F_{ext,z}(t))^T$ [N] and $\underline{M}_{ext,O}(t) = (M_{ext,O,x}(t), M_{ext,O,y}(t), M_{ext,O,z}(t))^T$ [N·m] are the total force and the total moment with respect to O, respectively, due to external effects acting on the ship at the generic time t.

In order to position and orient the vessel with respect to the earth-fixed reference system, dynamic equation (1) are supplemented by kinematic relations linking the Euler angles ψ [rad] (yaw), ϑ [rad] (pitch) and ϕ [rad] (roll), and their derivatives, with the vectors $\underline{u}_O$ and $\underline{\omega}$. The order of rotations around ship-fixed coordinate axes is the common one used in Naval Architecture: first yaw, second pitch and finally roll. Defining the instantaneous position vector of O with respect to $\Sigma : \Omega\xi\eta\zeta$ as $\underline{\xi}_O(t) = (\xi_O(t), \eta_O(t), \zeta_O(t))^T$, and defining the vector of Euler angles as $\underline{e}(t) = (\phi(t), \vartheta(t), \psi(t))^T$, the additional kinematics relations can be written as follows:

$$\begin{cases} \dfrac{d}{dt}\underline{\xi}_O = \underline{\underline{R}}_{S\to\Sigma}\underline{u}_O \\ \dfrac{d}{dt}\underline{e} = \underline{\underline{T}}_{\omega_S}^{-1}\underline{\omega} \end{cases} \tag{2}$$

The matrix $\underline{\underline{R}}_{S\to\Sigma}$ is the time dependent transformation matrix from S :

$Oxyz$ to $\Sigma : \Omega\xi\eta\zeta$, while the matrix $\underline{\underline{T}}_{\omega_S}^{-1}$ is the time dependent matrix which allows to transform the angular velocity expressed in components with respect to $S : Oxyz$ into derivatives of Euler angles. The explicit expressions for such matrices are as follows:

$$
\begin{cases}
\underline{\underline{R}}_{S\to\Sigma} = \underline{\underline{R}}_{\psi}\underline{\underline{R}}_{\vartheta}\underline{\underline{R}}_{\phi} = \begin{pmatrix} r_{11} & r_{12} & r_{13} \\ r_{21} & r_{22} & r_{23} \\ r_{31} & r_{32} & r_{33} \end{pmatrix} \\
\underline{\underline{T}}_{\omega_S}^{-1} = \begin{pmatrix} 1 & \sin(\phi)\tan(\vartheta) & \cos(\phi)\tan(\vartheta) \\ 0 & \cos(\phi) & -\sin(\phi) \\ 0 & \sin(\phi)/\cos(\vartheta) & \cos(\phi)/\cos(\vartheta) \end{pmatrix} \\
\text{with:} \\
\underline{\underline{R}}_{\psi} = \begin{pmatrix} \cos(\psi) & -\sin(\psi) & 0 \\ \sin(\psi) & \cos(\psi) & 0 \\ 0 & 0 & 1 \end{pmatrix} \\
\underline{\underline{R}}_{\vartheta} = \begin{pmatrix} \cos(\vartheta) & 0 & \sin(\vartheta) \\ 0 & 1 & 0 \\ -\sin(\vartheta) & 0 & \cos(\vartheta) \end{pmatrix} \\
\underline{\underline{R}}_{\phi} = \begin{pmatrix} 1 & 0 & 0 \\ 0 & \cos(\phi) & -\sin(\phi) \\ 0 & \sin(\phi) & \cos(\phi) \end{pmatrix} \\
r_{11} = \cos(\psi)\cos(\vartheta) \\
r_{12} = \cos(\psi)\sin(\phi)\sin(\vartheta) - \cos(\phi)\sin(\psi) \\
r_{13} = \sin(\phi)\sin(\psi) + \cos(\phi)\cos(\psi)\sin(\vartheta) \\
r_{21} = \cos(\vartheta)\sin(\psi) \\
r_{22} = \cos(\phi)\cos(\psi) + \sin(\phi)\sin(\psi)\sin(\vartheta) \\
r_{23} = \cos(\phi)\sin(\psi)\sin(\vartheta) - \cos(\psi)\sin(\phi) \\
r_{31} = -\sin(\vartheta) \\
r_{32} = \cos(\vartheta)\sin(\phi) \\
r_{33} = \cos(\phi)\cos(\vartheta)
\end{cases}
\tag{3}
$$

In SHIXDOF, the system (1)–(3) can be integrated in time with different numerical schemes. In the present work, a 4th order Adams-Bashforth scheme is used, in order to allow the setting-up of the co-simulation strategy described later in section 2.3. The considered integration scheme is an explicit one and it is characterised by a constant time step.

According to (1), the interaction of the vessel with the external world is modelled by means of $\underline{F}_{ext}(t)$ and $\underline{M}_{ext,O}(t)$. Such effects typically comprise the interaction with surrounding fluid, propulsors, rudders, moorings, etc. (Bulian and Francescutto, 2013; Bulian et al., 2012). For each considered physical phenomenon, a specific (simplified) model is considered, and this is the reason why, as said, the simulation approach is of the system-based type. In the following, different sub-models are described concentrating on those which are more relevant for the example application reported herein. In the following, the term "forces" is used in a generalised way, to indicate both forces and moments.

Forces due to Froude-Krylov pressure (herein the term "Froude-Krylov" indicates the total pressure, comprising both the hydrostatic term and the disturbance due to the presence of waves) are calculated considering the instantaneous wetted surface of the hull. This is a fundamental characteristic in order to be able to simulate phenomena which are driven by geometrical nonlinearities (e.g. parametric roll and nonlinear rolling in beam waves). To have a pressure field defined in the domain below the actual free surface, a stretching of the linear Airy theory is used, along the line of Wheeler (1969). The stretching is performed guaranteeing zero pressure at the free surface. Also, the stretching involves both the pressure field as well as the field of wave particle velocities. In order to determine the forces, the ship hull is represented by a mesh made of triangular panels, and the contribution of each panel to the total forces is determined by a zero-th order integration based on the calculation of pressure at the centre of the panel.

Potential added mass and damping forces are implemented in such a way that associated radiation effects can be taken into account under general motions. To this end the implementation is based on convolution integrals (Bailey et al., 1998; Cummins, 1962). Kernel functions used in convolutions are determined from hydrodynamic coefficients (usually damping) coming from frequency domain linear hydrodynamic pre-calculations. The linear pre-calculations can be either 2D (strip--theory) or 3D, according to the available pre-processor. Infinite frequency added masses, which are added to the global rigid body mass matrix, can be either directly provided or can be estimated from the hydrodynamic coefficients. Also instantaneous diffraction forces are determined from frequency domain data coming from linear hydrodynamic pre-calculations. However, in this case, a transfer function approach is used. At each time instant, the contribution to the total diffraction force from each wave component is determined from frequency domain data considering the instantaneous heading of the vessel, and the instantaneous position (and thus phase) of the vessel with respect to the considered wave component. The contributions from all the waves representing the sea elevation are eventually summed up to get the total diffraction force.

Manoeuvring forces are determined combining a lift model and a cross flow-model. The need for combining a lift model and a cross-flow model comes from the fact that in blended 6-DOF codes allowing the simulation of manoeuvring in waves, as it is the case of the code used herein, the manoeuvring sub-model could need to be used at large drift angles. Such models are intended to work in waves, and are typically derived as extension of models for calm water manoeuvring simulation. However, the large drift angles condition is a condition which standard manoeuvring models, developed for small drift angles, cannot cope with (see, e.g., Oh and Hasegawa, 2013; Sinibaldi and Bulian, 2014). To allow simulations at large drift angles, it is therefore often necessary to have a modified linear manoeuvring model coupled with a cross-flow model (e.g. Faltinsen, 1993; Toxopeus, 2006). The former is intended to provide forces at small drift angles, while the latter is intended to provide drag-based forces and moments particularly at large drift angles. In SHIXODF, linear manoeuvring forces due to lift effects are accounted for by means of a derivative-based approach. As a standard, derivatives from Clarke et al. (1983) are used, but such coefficients can of course be substituted by more accurate specific values, when available. Coupling with roll is introduced by assuming that the transversal force is acting at the geometrical centre of the underwater portion of the ship centreplane. A progressive reduction of lift forces at large drift angles is also considered to avoid unrealistic predictions of forces. The spatial variability of flow field due to wave induced orbital velocities is accounted for in the lift manoeuvring sub-model by using an "equivalent surge-yaw-sway motion" relative to the water, similarly to Artyszuk (2006). It is interesting to note that this idea is to some extent similar to that used by Greco and Lugni (2012) and Greco et al. (2014), although therein it was applied to convolution terms leading to radiation and diffraction forces under the weak-scatterer hypothesis. In order to determine forces also in the range of large drift angles, and to be so able to deal with large drift angle manoeuvres, a cross-flow model supplements the described lift model. Forces coming from the cross-flow model are calculated by determining the average relative velocity between the vessel and the (undisturbed) surrounding wave field at different panels distributed on the ship centreplane. Making use of a local drag coefficient, and of the local squared relative velocity, each panel contributes to the global force, and a final summation allows to determine the global cross-flow force. It is worth noting that this automatically generates also a roll moment associated with the cross-flow model. The described panelised approach is basically a slight generalization of the more classical sectional approach for modelling cross-flow in case of ships manoeuvring in calm water and in waves (e.g. Hughes et al., 2011; de Kat and Paulling, 1989).

Although different sub-models naturally contribute to roll damping (linear radiation model, manoeuvring model, aerodynamic model when air is taken into account), the resulting roll damping very seldom matches the desired (experimental or predicted) value. To cope with this fact, additional linear and nonlinear roll damping coefficients can be introduced for tuning purposes, and a dependence on forward speed can also be considered.

The (longitudinal) calm water resistance of the vessel is modelled by

means of a pre-computed speed-resistance curve. At each time instant the average relative forward speed between the ship and the water (accounting for wave particles velocities, if necessary) is determined, and the corresponding longitudinal resistance force is interpolated.

Springs can be introduced to limit certain motions which do not have natural restoring (surge, sway and yaw – this latter when in absence of steering). This is typically necessary in order to avoid hardly controllable undesired low frequency motions. In some cases springs can also be useful to approximately reproduce some specific experimental conditions. A typical case are experiments in beam waves, when the vessel is manually adjusted to keep an almost 90deg heading. In such case, springs based on the yaw motion and generating a corresponding yaw moment allow to (approximately) keep the desired condition.

Other sub-models are available to represent the effect of other external actions, such as lifting surfaces (e.g. rudder, anti-rolling fins), propulsors, wind and in general aerodynamic effects, linear/nonlinear elastic mooring lines, etc. Such models, however, are not relevant for the present study.

In addition, to the above, in order to allow the co-simulation which is the scope of this study, $\underline{F}_{ext}(t)$ and $\underline{M}_{ext,O}(t)$ also contain the total force and moment generated on the ship by the fluid in the tank. Such interaction force and moment are coming from the coupling with the tank flow solver, which is described in the next section.

2.2. Internal flow

The SPH solver used in this work is AQUAgpusph (Cercos-Pita, 2015; Cercos-Pita et al., 2013). Such solver is based on the WC-SPH methodology, one of the most popular mesh-free methods in Computational Fluids Dynamics (CFD). WC-SPH has demonstrated to be ideally suited to carry out simulations where complex geometries are considered and also when complex, non-single valued, free surface dynamics dominate the flow (see Bouscasse et al., 2013, 2014a,b; Monaghan, 2005, 2012). In this model the fluid domain is discretised in particles which are treated from a Lagrangian point of view, such that the properties of these particles are attributed to their centres. Then, defining a convenient kernel function $W[\mathrm{m}^{-3}]$, the following convolution integral for a generic field f, in discrete form, is used:

$$\langle f\rangle_i = \frac{1}{\gamma_i}\sum_{j\in\mathrm{Fluid}} f_j W_{ij}\frac{m_j}{\rho_j} \tag{4}$$

In the previous expression m_j [kg] and ρ_j [kg/m^3] are the mass and density of a generic particle j, and γ_i [−] is a renormalization factor defined as follows:

$$\gamma_i = \sum_{j\in\mathrm{Fluid}} W_{ij}\frac{m_j}{\rho_j} \tag{5}$$

The same convolution (4) can be used to approximate the gradient of a generic field as well:

$$\langle\nabla f\rangle_i = \frac{1}{\gamma_i}\left(\sum_{j\in\mathrm{Fluid}} f_j\nabla_i W_{ij}\frac{m_j}{\rho_j} + \sum_{j\in\mathrm{Boundary}} f_j\underline{n}_j W_{ij}s_j\right) \tag{6}$$

where the divergence theorem has been applied. In the previous equation s_j [m^2] and $\underline{n}_j$ [−] are the area and the unit normal vector of the generic boundary element j. Traditionally, the summation over the boundary elements has been replaced by a summation over fluid extension particles, such that their properties can be conveniently set to enforce the desired boundary condition. However, in the last years the possibility of keeping the last boundary integral term is attracting the interest of the researchers (see Cercos-Pita, 2015; Ferrand et al., 2013; Macià et al., 2012), since this formulation allows to handle complex geometries in a more natural and easier way. The main feature of formulation (6) is that it allows to approximate the gradient of the field f, for a generic particle i, using only the already known properties of the surrounding particles, hereinafter refereed as neighbours. Therefore, using such approximation, the WC-SPH numerical scheme reads as follows:

$$\begin{cases} \dfrac{d\rho_i}{dt} = -\rho_i\langle\nabla\cdot\underline{u}\rangle_i \\ \dfrac{d\underline{u}_i}{dt} = -\dfrac{\langle\nabla p\rangle_i}{\rho_i} + \dfrac{1}{\rho_i}\langle\nabla\cdot\underline{\underline{T}}\rangle_i + \underline{g} \\ \dfrac{d\underline{r}_i}{dt} = \underline{u}_i \\ p_i = c_0^2(\rho-\rho_0) \end{cases} \tag{7}$$

where $\underline{r}_i$ [m], $\underline{u}_i$ [m/s] and p_i [Pa] are the position, velocity and pressure of a generic particle i, c_0 [m/s] is the speed of sound of the fluid, $\underline{g}$ [m/s^2] is the gravitational acceleration, and $\underline{\underline{T}}$ [Pa] is the stress tensor. However, for conservation and consistency reasons, the approximation of the differential operators is not performed applying directly the expression (6), but using the so-called symmetrised operators (see Colagrossi et al. (2009) and references therein) defined as follows:

$$\rho_i\langle\nabla\cdot\underline{u}\rangle_i = \frac{1}{\gamma_i}\sum_{j\in\mathrm{Fluid}}(\underline{u}_j-\underline{u}_i)\cdot\nabla_i W_{ij}m_j + \frac{1}{\gamma_i}\sum_{j\in\mathrm{Solid}}(\underline{u}_j-\underline{u}_i)\cdot\underline{n}_j W_{ij}\rho_j s_j \tag{8}$$

$$\frac{\langle\nabla p\rangle_i}{\rho_i} = \frac{1}{\gamma_i}\sum_{j\in\mathrm{Fluid}}\left(\frac{p_j}{\rho_j^2}+\frac{p_i}{\rho_i^2}\right)\nabla_i W_{ij}m_j + \frac{1}{\gamma_i}\sum_{j\in\mathrm{Solid}}\left(\frac{p_j}{\rho_j^2}+\frac{p_i}{\rho_i^2}\right)\underline{n}_j W_{ij}\rho_j s_j \tag{9}$$

$$\frac{1}{\rho_i}\langle\nabla\cdot\underline{\underline{T}}\rangle_i = \mu\sum_{j\in\mathrm{Fluid}}\frac{(\underline{u}_j-\underline{u}_i)\cdot(\underline{r}_j-\underline{r}_i)}{\rho_i\rho_j||\underline{r}_j-\underline{r}_i||^2}\nabla_i W_{ij}m_j \tag{10}$$

In AQUAgpusph equations (8)–(10) are integrated in time using an Improved Euler scheme. To this end the following time step is used:

$$\Delta t_{SPH} = C\frac{h}{c_0} \tag{11}$$

where C [−] is the Courant factor, which should be lower than one, and h [m] is the characteristic length of the kernel W . From (11) it can be appreciated that, in principle, considering the actual speed of sound in the fluid would lead to extremely small time steps. However, to alleviate this issue, for practical purposes, the actual speed of sound of the fluid is not usually used. Instead, a smaller value, fulfilling the following condition, is typically imposed:

$$c_0 > 10|\underline{u}|_{max} \tag{12}$$

where $|\underline{u}|_{max}$ [m/s] is the maximum speed expected in the flow. The speed of sound defined according to (12) (see also the equation of state in (7)) is large enough to assume that the density variations are very small and thus negligible for practical purposes. Unfortunately, the estimation of a reference limit value for the speed of sound is not a trivial task, as discussed by Marrone et al. (2015). For the specific study described herein, an indicative limit for the speed of sound can be selected considering a contribution coming from the maximum speed induced by ship motions at the tank location in absence of the tank ($|\underline{u}|_{sm,no-tank}$), plus a contribution linked with the maximum possible hydrostatic pressure in the upright position:

$$c_0 > \left(10|\underline{u}|_{sm,no-tank} + 10\sqrt{gH_T}\right) \tag{13}$$

where H_T [m] is the height of the tank.

The WC-SPH formulation described above results in a purely explicit numerical scheme. As a consequence, in order to guarantee the numerical stability of the scheme, either extremely small time steps should be used, or additional diffusion should be added. To this end, the δ-SPH diffusive term has been used in this work (see Antuono et al., 2012, 2015).

As it has been remarked above, the performance is a critical aspect for the tool described in this work. In this regard, AQUAgpusph is accelerated with OpenCL, allowing the usage of Graphics Processing Units (GPU) based devices (or, in general, any other accelerator) to obtain significant performance improvements compared to direct computations on Central Processing Units (CPU). However, to obtain such improvements, single precision computations should be used to perform the simulations, and this may cause precision issues. Domínguez et al. (2014) already demonstrated that in the cases where a large ratio between the distance between particles and the computational domain extensions is considered, precision issues may cause clamping of particles. However, due to the relatively low resolutions considered in this work, this problem has not become relevant. Unfortunately, the time integration is actually affected by precision issues, due to the extremely large ratio between the simulation time t and the small time steps Δt_{SPH} required by SPH. Hence, as it will be discussed later, the numerical scheme to interact with SHIXDOF has been designed using a relative time within each integration time step. In this way the global time t does not actually play a role in the formulation.

2.3. Co-simulation strategy

As previously discussed, the interaction between the SHIXDOF and AQUAgpusph is based on a co-simulation strategy (Cercos-Pita et al., 2015). In general, a co-simulation strategy can be divided in three main parts (e.g. Breuer et al., 2012; Elliott et al., 2006; Fleissner et al., 2010; Gomes et al., 2011):

1 The numerical scheme, or coupling;
2 The communication layer;
3 The implementation.

Details of these three parts for this specific application are described in the following.

2.3.1. Coupling

The possibility of developing tools to perform multi-physics coupled simulations is increasingly attracting the interest of the researchers in recent years. However, setting up the interaction between the different subsystems involved in a coupled simulation framework is itself a complex matter, which can be handled using different approaches. Felippa et al. (2001) reviewed the already existing techniques to design coupled approaches, classifying the approaches into: field elimination, monolithic or simultaneous treatment, and co-simulation or partitioned treatment.

The field elimination approach, which consists in the elimination of one or more fields, is restricted to special problems leading to linear systems which can then split in separate subsystems. Of course this approach cannot be applied for the coupling of the tools described in sections 2.1 and 2.2.

The monolithic or simultaneous treatment approach is based on the synchronous integration in time of the different subsystems. The main advantage of this approach is the stability. However, it has the drawback of being significantly intrusive in case already existing subsystems have to be coupled. As a consequence, this approach typically results in a more rigidly coupled system.

The co-simulation or partitioned treatment approach consists in treating each subsystem as an isolated entity, modelling the interactions as forcing effects that are communicated between the individual components. This type of co-simulation strategy is usually applied in case of so-called loosely coupled systems. Examples of loosely coupled systems are those where the interaction between two subsystems is achieved by communicating the interface force and displacement (see Elliott et al., 2006; Fleissner et al., 2010; Joosten et al., 2009; Sicklinger et al., 2014, and references therein), as it is the case in this study.

Using a co-simulation approach for the present application has a number of benefits. First, since both subsystems can use explicit time integration schemes, as it has been described in sections 2.1 and 2.2, the global system can be implemented using an explicit time integration scheme as well. Then, provided each subsystem has been separately optimized, maximum performance can be achieved if the interaction can be efficiently treated. Additionally, and importantly, the system can be modularized, allowing the addition of more instances of each subsystem (e.g. multiple tanks in a single ship).

As a result, a partitioned treatment of the problem has been chosen herein. In order to couple the two available tools during the time stepping, the Conventional Serial Staggered (CSS) purely explicit numerical scheme (see Farhat et al., 2006) has been used. For the specific application reported herein, such integration scheme is depicted in Fig. 1.

The flow shown in Fig. 1 can be therefore summarized as follows:

1. AQUAgpusph sends the interpolated force $\underline{F}_{ext}(t_N)$ and moment $\underline{M}_{ext,O}(t_N)$ to SHIXDOF, where O denotes the centre of ship-fixed reference system;
2. SHIXDOF advances in time by Δt while AQUAgpusph is waiting;
3. SHIXDOF sends the time step Δt and the new motions at time t_{N+1} to AQUAgpusph, comprising the new coordinates of the reference point O in the earth-fixed reference system, the attitude of the ship-fixed reference system using Euler angles (ϕ - roll, ϑ - pitch, ψ -yaw), and the associated instantaneous time derivatives;
4. Finally, AQUAgpusph advances in time by Δt as well, but using a different time step, Δt_{SPH}. Ship motions within the time interval $[t_N, t_{N+1}]$ are determined by AQUAgpusph through an interpolation procedure. During this process SHIXDOF is waiting at $t_{N+1} = t_N + \Delta t$ for the force $\underline{F}_{ext}(t_{N+1})$ and moment $\underline{M}_{ext,O}(t_{N+1})$, in order to start the next time step.

For starting the time stepping, the calculation of forces at $t = 0$ in AQUAgpusph is done by assuming that the vessel starts from rest, which is actually the case in the simulations carried out herein.

Since SHIXDOF uses a time step much longer than AQUAgpusph's ($\Delta t \sim 10^2 \Delta t_{SPH}$), it is necessary for AQUAgpusph to have information regarding the motions inside the interval $[t_N, t_{N+1}]$. To this end, 3rd order polynomial interpolations of the coordinates of the reference point (O) and of the Euler angles (ϕ, ϑ, ψ) are constructed by using the values of the variables, and the corresponding derivatives, at t_N and t_{N+1}.

The large ratio between the time steps Δt and Δt_{SPH} can induce aliasing in the forces received by SHIXDOF, whenever the forces computed by AQUAgpusph contains high frequencies fluctuations. In order to reduce this effect, a Linear Least Squares (LLS) fitting on the force $\underline{F}_{ext}(t)$ and moment $\underline{M}_{ext,O}(t)$ computed by AQUAgpusph is performed between t_N and t_{N+1}. Furthermore, this is also helping in reducing the noise in the

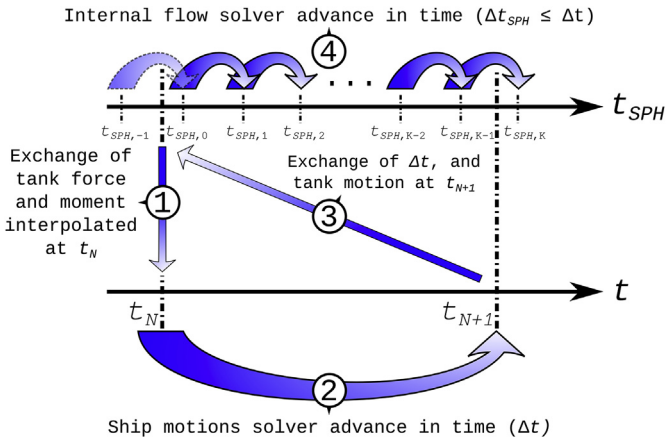

Fig. 1. Implemented time stepping algorithm, based on Conventional Serial Staggered (CSS) purely explicit numerical scheme. The indices enclosed by circles denote the order of processes.

force and moment inherently resulting by the application of the WC-SPH methodology. It is noted that, from tests carried out at development stage, the described LLS filter is not introducing undesired artifacts in the signal received by SHIXDOF.

According to the described integration scheme (Fig. 1), the only condition which need to be fulfilled regarding time steps is that $\Delta t_{SPH} \leq \Delta t$. Concerning ratios between time steps, it is not necessary that Δt is a multiple of Δt_{SPH} thanks to the interpolation procedure described above.

It is also noted that when constant time step integration schemes are used for the ship motions solver, as in the present case, passing Δt at each communication is redundant. However, exchanging this information provides flexibility for implementation of variable time step integration schemes where Δt is no longer necessarily constant.

2.3.2. *Communication layer*

Once the numerical scheme has been defined, a two-way channel between the subsystems should be provided in order to exchange the necessary information. Due to the nature of both applications, the communication between the codes can be achieved: through a dynamic linking, through an intermediate program or file, or through a network connection.

The dynamic linking alternative is the most efficient one. However, it has some drawbacks that should be considered. In fact, in such a case, both tools should be launched in the same system, introducing a dependency on the platform. Furthermore, in case of simulations considering multiple tanks, the number of tanks would be limited by the hardware of the system where the simulation is run. Differences in code implementation languages, as in the present case, could further complicate the coupling, by requiring the creation of, e.g., specific wrappers.

The communication through intermediate program or files has similar disadvantages compared to the dynamic linking, with the addition of being less efficient and less robust. In general it is chosen as an alternative to the dynamic linking, when this latter cannot be applied, for instance due to licensing issues.

Among the three alternatives, the linking through a network connection is better suited to exploit all the benefits of the partitioned treatment discussed in section 2.3.1. Indeed, an exchange of data based on network communication is much less intrusive and potentially more scalable. Hence, in the present application, a communication based on network connection is used. Considering the fact that a relatively low amount of data is exchanged in this application, the communication is based on TCP/IP connection (e.g. Comer, 2013) and the architecture is setup having a GRID paradigm (e.g. Foster et al., 2008) in mind, i.e. a virtual platform of coordinated resources in a multi-institutional virtual organization where, potentially, an arbitrary number of servers equipped with AQUAgpusph can be deployed as on-demand service providers for SHIXDOF clients.

2.3.3. *Implementation*

In order to finalise the co-simulation strategy, both the numerical scheme discussed in section 2.3.1 and the communication channel chosen in section 2.3.2 should be joined in a common implementation. Fig. 2 schematically shows the co-simulation implementation.

From Fig. 2 it can be appreciated that such strategy relies on three main actors: SHIXDOF (acting as client), Daemon (acting as a server manager and simulation generator), AQUAgpusph, (the computational part of the server). The working flow of each simulation can be briefly summarized as follows:

1. At first, an initialization phase is carried out, where SHIXDOF sends the simulation data to the Daemon, which is responsible for setting up the simulation, for launching AQUAgpusph and for sending back to SHIXDOF a small report containing the initialization results.
2. After the system has been initialized, the control of the server is assigned to AQUAgpusph, which runs a couple of seconds without motions, as a stabilization technique, in order to avoid shocks in the initial forces. Afterwards SHIXDOF establishes a new connection, which will then be used throughout the simulation, with AQUAgpusph.
3. Eventually, the actual coupled simulation can start by carrying out the time stepping loop, following the numerical scheme described in section 2.3.1.

3. Application

An example application of the developed co-simulation tool has been carried out using a freely available and well-known hull form geometry. The choice of the geometry was based on two main considerations. Firstly, using the selected geometry allows present results to serve as possible comparison cases for other researchers developing similar tools. Secondly, the considered hull has been selected also because experimental data regarding nonlinear rolling motion without tank were available from previous studies, and such type of data represent a valuable set of information for the tuning of the roll damping model in the blended ship motions code.

Although experimental tests have not been carried out herein for the hull equipped with the tank, the geometry and positioning of the tank in the simulations were chosen in such a way to be compatible with an already existing 1:100 scale model of the hull. Scope of this choice was to ease possible future experimental developments aimed at validating the simulations. As a result of such choice, the position of the tank in the simulations is quite high above the waterline and above the centre of gravity.

A series of simulations have been carried out in regular beam waves considering two main simulation parameters: the longitudinal extent of the tank, and the steepness of the waves. The filling level of the tank has been selected in order to let the tank working as an anti-rolling device. The reasons for considering a setup where the tank can work as an anti-

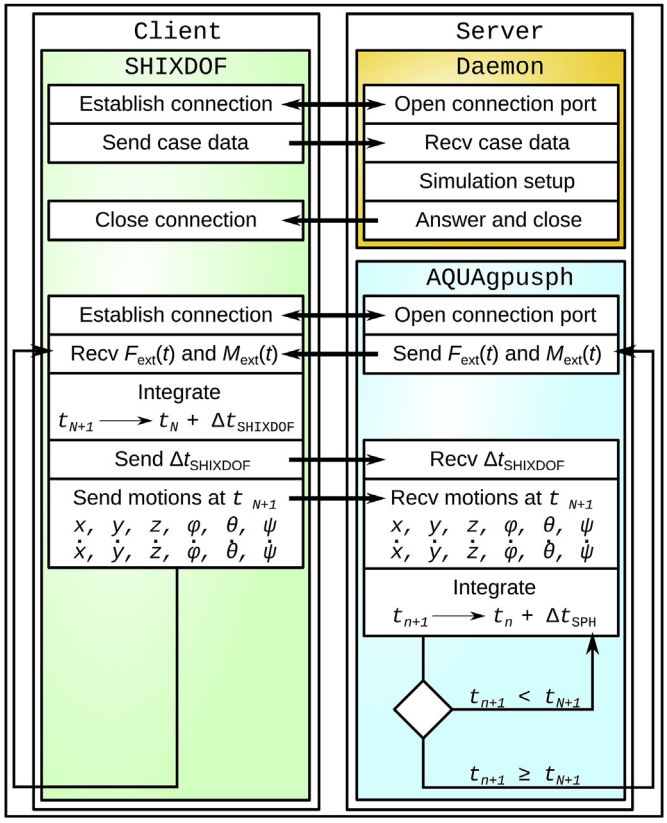

Fig. 2. Implementation of the co-simulation strategy.

Table 1
Main parameters of Series 60 hull and main data of loading condition without tank as used for simulations.

Length between perpendiculars - L_{BP}	[m]	162.5	Transversal metacentric height – $\overline{GM}$	[m]	1.65
Breadth – B	[m]	25.0	Height of centre of gravity above baseline – $\overline{KG}$	[m]	8.59
Draught – T	[m]	10.0	Roll natural frequency - ω_0	[rad/s]	0.408
Height of deck from baseline – H_{deck}	[m]	20.0	Dry roll radius of inertia w.r.t. CoG – $R_{xx,G}$	[m]	9.1
Block coefficient – C_B	[−]	0.8	Dry pitch radius of inertia w.r.t. CoG – $R_{yy,G}$	[m]	40.6
Height of transversal metacentre above baseline – $\overline{KM}$	[m]	10.24	Dry yaw radius of inertia w.r.t. CoG – $R_{zz,G}$	[m]	40.6
Coordinate of mid perpendicular – x_{MP}	[m]	81.25	$R_{xx,G}/B$	[−]	0.364
Length-breadth ratio – L_{BP}/B	[−]	6.5	$R_{yy,G}/L_{BP}$	[−]	0.250
Breadth-draught ratio – B/T	[−]	2.5	$R_{zz,G}/L_{BP}$	[−]	0.250

rolling device are, on the one side, because this is the condition where, typically, the most relevant coupling arises from a dynamical perspective, and, on the other side, because this is a setup which is potentially relevant for safety aspects associated with the reduction of roll motion at sea. Considering different lengths of the tank was aimed at assessing the effect of different mass-ratios (ratio between the mass of the anti-rolling tank and the mass of the ship) on the roll response curve. Furthermore, simulations with different tank lengths allowed to select a specific length of the tank for the analysis considering different wave steepnesses. Scope of this latter analysis was the assessment of nonlinear effects on the roll motion, coming from the combination of external hydrodynamics (ship-wave interaction) and internal hydrodynamics (ship-tank interaction).

In the coupled simulations, SHIXDOF was running on a computer at the University of Trieste, while AQUAgpusph was running on a computer at the Technical University of Madrid.

In the following, the hull and tanks geometry are firstly described. Afterwards, results from the tuning of the ship motions code on available experimental data are reported. The effect of changing the longitudinal extent of the tank is discussed next. The analysis of roll behaviour for different forcing amplitudes and one specific tank length is then presented and discussed, showing the appearance of clearly nonlinear effects. Some considerations regarding simulation performances are finally provided.

For validation purposes of the coupled code, another case is instead considered separately in the Appendix. Specifically, in the Appendix, simulations are carried out for the case reported by de Kat (2000), using the same simulation methodology presented, more extensively, in the present section. The hull used in the Appendix is a 200kDWT tanker equipped with a free surface tank, for which model tests were carried out with and without a partially filled tank, in regular beam waves, and for which both roll and heave motions were measured and reported by de Kat (2000). The Appendix firstly reports a discussion on the available input data from de Kat (2000) with reference to the input data eventually used for the simulations. Then, a description of the code tuning process, based on the hull without partially filled tank, is reported, in line with the approach described in the present section. Finally, simulated and experimentally measured roll and heave motions of the tested 200kDWT tanker are compared, for both the cases of ship with and without partially filled tank. The comparisons show an overall satisfactory agreement between simulations and experiments in both conditions, thus validating the approach used herein. More details regarding the validation are reported in the Appendix.

3.1. Hull and tanks geometry

In order to provide data related to a freely available hull geometry, the hull used in the example simulation is a Series 60 (Todd et al., 1957). Table 1 reports the main characteristics of the hull and of the loading condition without tank. The same hull form was used in the past, without any tank onboard, for experimental tests in regular and irregular beam waves (Bulian et al., 2012; Bulian and Francescutto, 2013). The height of the deck reported in Table 1 corresponds to the upper limit of the available scaled model.

For carrying out numerical simulations, three different tank geometries have been considered. In all the three cases the tank is box shaped, longitudinally positioned amidships, with a fixed height H_T of 5 m, and a breadth B_T equal to the ship breadth. The three considered configurations differ in the longitudinal extent L_T of the tank. The main characteristics of the considered tanks and the main effects on the ship loading condition and initial stability are reported in Table 2. A front view of hull sections and tanks geometry is shown in Fig. 3, while a side view of the centreplane is shown in Fig. 4. In Table 2, the tank-mass ratio is the ratio between the mass of the fluid in the tank and the mass of the vessel in the loading condition specified in Table 1, considering the same density for external water and water in the tank. Table 2 also reports the increase of draught, with respect to the condition in Table 1, due to the loading of the fluid in the tank. For simplicity and for ease of comparison of outcomes, in this study it is assumed that the hull without tank has the same mechanical properties (mass, position of centre of gravity, radii of inertia) of the hull equipped with the empty tank. As a result, the indications “without tank” and “empty tank” are to be assumed, hereinafter, as synonymous. Since the interest in this example application is on the behaviour of the coupled system when the tank is designed to act as an anti-rolling device, the depth d_{fluid} of the fluid inside the tanks has been selected in such a way that the natural frequency of the first linear transversal sloshing mode, $\omega_{1,SL}$ [rad/s], matches the roll natural frequency of the vessel without tank. The expression for $\omega_{1,SL}$ is (e.g. Faltinsen and Timokha, 2009):

$$\omega_{1,SL} = \sqrt{g\frac{\pi}{B_T}tanh\left(\frac{\pi}{B_T}d_{fluid}\right)} \tag{14}$$

where g $[m/s^2]$ is the gravitational acceleration.

Looking at the data in Table 2 it can be noticed that the tank-ship mass ratio for the three considered configurations is small, and small is also the corresponding increase of ship draught due to the loading of fluid in the tank. It is also important to notice that the ratio between the fluid depth and the tank breadth is 4.32%. As a result, the fluid dynamics in the tanks is characterised by a shallow water regime. In this respect, it is worth noting that results from the work by Bouscasse et al. (2013), which reports comparison of numerical WC-SPH simulations and experimental sloshing data under small to large amplitude sway motions, indicate that WC-SPH can be effectively used in shallow water conditions.

The static effect of the tank on the overall restoring capabilities of the vessel is analysed by calculating the righting lever curve $\overline{GZ}$ [m] in the considered configurations. Results of the calculations are shown Fig. 5. Due to the fact that the fluid in the tank is loaded above the centre of gravity of the vessel without tank, part of the roll restoring reduction is due to the shift of the (solid) global centre of gravity, while the remaining reduction of the restoring is due to the free surface effect, i.e. the shift of fluid as the ship heels. For small heeling angles the part of restoring reduction due to the variation of the vertical position of the centre of gravity is associated with the variation between the metacentric height with empty tank (see Table 1) and the metacentric height with “frozen” liquid (see Table 2), while the contribution of the free surface effects to small angles restoring can be seen by comparing $\overline{GM}_{solid}$ and $\overline{GM}_{fluid}$ in Table 2. Part of the change in $\overline{GZ}$ when loading the fluid in the tank is also to be attributed to the change of ship draught. However, since this change

Table 2
Main characteristics of the tanks and main effects on ship loading condition and initial stability.

Longitudinal extent – L_T	[m]	5.0	10.0	20.0
Transversal extent – B_T	[m]	25.0	25.0	25.0
Height – H_T	[m]	5.0	5.0	5.0
Longitudinal position of the centre of the tank	[m]	81.25 (corr. to amidships)	81.25 (corr. to amidships)	81.25 (corr. to amidships)
Vertical position of tank bottom from ship bottom	[m]	22.0	22.0	22.0
Fluid depth – d_{fluid}	[m]	1.08	1.08	1.08
Frequency of first linear transversal sloshing mode – $\omega_{1,SL}$	[rad/s]	0.408	0.408	0.408
Tank filling ratio	[%]	21.6	21.6	21.6
Fluid depth-tank breadth ratio – d_{fluid}/B_T	[-]	0.0432	0.0432	0.0432
Tank-ship mass ratio	[%]	0.42	0.83	1.66
Increase of ship draught from T=10m	[m]	0.038	0.076	0.151
Height of centre of gravity (ship + tank) above baseline – $\overline{KG}$	[m]	8.65	8.70	8.82
Metacentric height with "frozen" liquid - $\overline{GM}_{solid}$	[m]	1.59	1.53	1.42
Metacentric height corrected for free surface effects - $\overline{GM}_{fluid}$	[m]	1.39	1.13	0.63
Stabilizer size coefficient - $\mu_{tank} = (\overline{GM}_{solid} - \overline{GM}_{fluid})/\overline{GM}_{solid}$	[-]	0.13	0.26	0.56
Stabilizer capacity η_{tank}	[rad]	0.0255	0.0526	0.1111

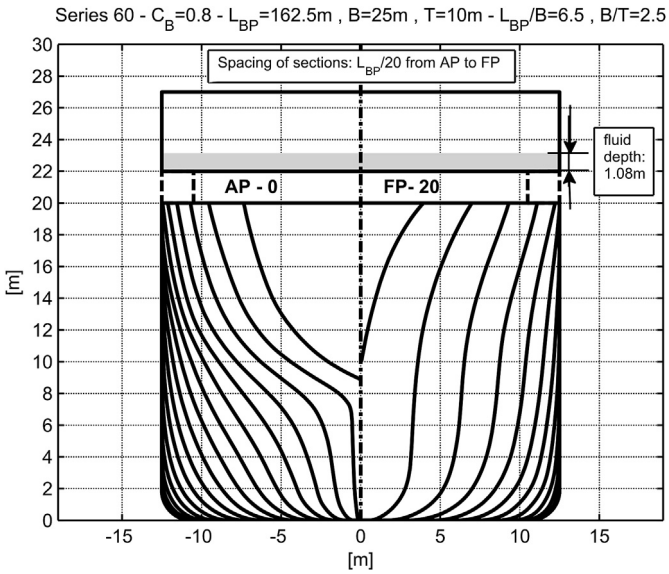

Fig. 3. Front view of hull sections and tanks geometry.

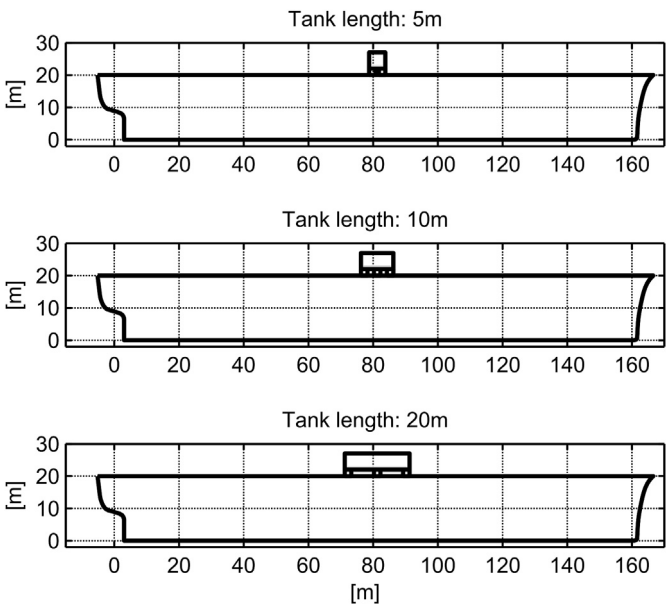

Fig. 4. Side view of hull and tanks geometry at ship centreplane.

of draught is small (see Table 2), the corresponding effect on $\overline{GZ}$ is small as well.

Looking at Table 2 it is also useful to report a note regarding the ship-tank tuning. Indeed, the depth of the fluid was chosen by setting $\omega_{1,SL}$ equal to the roll natural frequency of the vessel without tank, leading to a reference nominal stabilizer tuning factor $\omega_{1,SL}/\omega_0 = 1.00$ (Beck et al., 1989). When the fluid is loaded onboard, however, the actual stabilizer tuning factor is modified as a consequence of the different mass distribution. A new stabilizer tuning factor should therefore be determined with respect to the roll natural frequency of the vessel with "frozen" liquid. Assuming that the roll natural frequency in such condition is approximately proportional to $\sqrt{\overline{GM}_{solid}}$, it turns out that the stabilizer tuning factor for the three considered tank lengths would be approximately 1.02, 1.04 and 1.08 for the three lengths of 5 m, 10 m and 20 m, respectively. The estimated variation is therefore small, and does not lead to any strong detuning of the anti-rolling tank. On the contrary, according to Beck et al. (1989), a stabilizer tuning factor slightly larger than unity leads to a more effective anti-rolling tank.

Table 2 also reports two additional parameters, as defined by Beck et al. (1989). The first parameter is the "stabilizer size" coefficient, herein indicated as μ_{tank}. It can be seen that, for the three considered tank lengths, μ_{tank} ranges from 0.13 to 0.56. According to Beck et al. (1989), typical good designs of stabilizers have μ_{tank} of around 0.20. Although it is not the scope of this study to provide a design of an anti-rolling tank, it is however worth reporting that, for the configuration considered herein, a

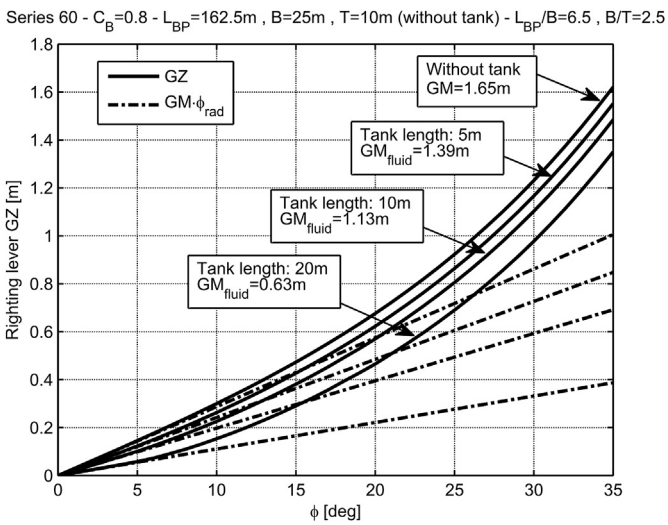

Fig. 5. Righting lever curve of the vessel in the considered configurations.

value of $\mu_{tank} = 0.20$ would be achieved by a tank length of about 7.85 m. The second parameter is the "stabilizer capacity", herein indicated as η_{tank}, which represents the maximum heel to which the stabilizer can heel the ship assuming all the fluid to be placed on one side of the tank. In the calculation of η_{tank} the fluid has been considered to occupy the whole height of the tank, and to be placed at the extreme side of the tank. According to Beck et al. (1989), a stabilizer loses effectiveness when the effective wave slope is larger than η_{tank}. The results reported later in the paper will therefore be discussed also with reference to this parameter. It is worth noting here that the three values of η_{tank} reported in Table 2 correspond to effective wave steepnesses of 1/123, 1/60 and 1/28, for tank lengths of 5 m, 10 m and 20 m, respectively. The phenomenon of reduction of effectiveness of free surface anti-rolling tanks was also discussed by Carette (2015) from the point of view of reduced damping effect as the rolling amplitude increases, in contrast to the typical opposite effect of more common passive anti-rolling devices, such as bilge-keels, which instead become more effective as the rolling amplitude, and thus roll velocity, increases.

3.2. Tuning of ship motion code

Blended nonlinear ship motions codes always require a certain tuning before it is possible to reliably use them for prediction purposes. The necessity of tuning comes from the fact that such types of codes, as already said, are of the system-based type. This means that they are based on sub-models which have a partially semi-empirical nature and which usually rely on specific parameterizations. In general the tuning process depends on the intended use, because the sensitivity of results to the parameters of each sub-model depends on the specific application. When roll motion is of concern, it is almost invariably necessary to properly tune roll damping coefficients in relevant sub-models. Such tuning is necessary in order to provide a simulated dissipation which is in line with the reality.

Different sub-models typically contribute, implicitly, to roll dissipation (linear hydrodynamics, manoeuvring forces due to lift, cross-flow). However the combination of basic sub-models usually does not allow to match roll damping as observed from, e.g., experimental roll decays. For such reason additional semi-empirical damping coefficients are typically used in the tuning process of blended codes in order to add further dissipation in the form of a roll moment proportional to the roll velocity (linear roll damping) or the square/cube of the roll velocity (quadratic and cubic roll damping, respectively).

A typical way of tuning roll damping coefficients is by starting from roll decay data. The tuning procedure, indeed, often starts from an analysis of roll decay experiments, in order to determine the reference amplitude dependent linear equivalent roll damping coefficient (Himeno, 1981). In absence of experimental data, semi-empirical prediction methods (e.g. Blume, 1979; Kawahara et al., 2009) or CFD-based roll decay simulations (e.g. Broglia et al., 2009; el Moctar et al., 2012; references in Bačkalov et al. (2016)), can be used as a reference target. Then, simulated roll decays are performed using the blended code, and the tuning coefficients in the sub-model(s) of the blended code are modified, in such a way that the analysis of simulated roll decays leads to an amplitude dependent equivalent linear roll damping coefficient which is as close as possible to target data.

However, when experimental data regarding forced roll motion in waves are available, such initial tuning of roll damping can be further improved by a fine tuning intended to lead to a better matching of forced roll simulations and experimental results. Of course, a direct tuning can also be done using forced roll motion data without passing through roll decays.

In line with the described tuning process, and before carrying out the intended set of coupled ship-tank simulations, the 6-DOF code has therefore been tuned using available experimental data regarding roll decays and forced roll in regular beam waves at zero forward speed (Bulian and Francescutto, 2013; Tzamtzis, 2004) for two wave steepnesses s_W (ratio between wave height and wave length): $s_W = 1/100$ and $s_W = 1/30$. In a previous work (Bulian and Francescutto, 2013), roll motion in beam regular waves was simulated using roll damping tuned solely on roll decays, and the resulting simulated roll motion amplitude was slightly larger than the experimental one at the largest tested forcing wave steepnesses for the loading condition considered in the present work. Herein, further tuning of the roll damping model has been undertaken, aiming at achieving a better matching with experimental data at large forcing wave steepnesses, while still keeping a good matching with roll decay data and experiments in milder waves. In the tuning process, the drag coefficient used in the cross flow model has been kept constant to a value equal to 0.8, which is in line with typical lateral drag coefficients for quite full vessels with similar beam to draught ratios (e.g. Faltinsen, 1993; Kijima, 2003). From the analysis of the behaviour of roll decays, the tuning of damping was carried out by means of an additional empirical linear-in-velocity term ($-B_{L,add}\dot{\phi}$) and an additional cubic-in-velocity term ($-B_{C,add}\dot{\phi}^3$), generating damping moments acting along the ship longitudinal axis passing through the centre of the ship-fixed reference system, which is placed amidships, on the centreplane and at a height above the bottom corresponding to the calm water ship draught. From the tuning process, the additional linear and cubic damping coefficients, for the considered selection of the ship-fixed reference system, were set to $B_{L,add} = 2.1{\cdot}10^7 N{\cdot}m/(rad/s)$ and $B_{C,add} = 3.0{\cdot}10^9 N{\cdot}m/(rad/s)^3$, respectively. Such re-tuning has eventually led to a reduction in the difference between experiments and simulations for the maximum roll response at the larger steepness, from about 15% in Bulian and Francescutto (2013) to about 9% herein. The difference in peak at the lowest steepness was instead kept at about 2%.

Results from the tuning, in terms of comparison between experimental data (transformed to full scale) and simulations, are reported in Fig. 6. As anticipated, experimental tests reported in the figure were carried out in beam regular waves with two wave steepnesses, namely $s_W = 1/100$ and $s_W = 1/30$. During the experiments, which were conducted at the Hydrodynamic Laboratories of the University of Trieste, the model was free to drift under the action of waves. The heading was manually controlled by means of ropes connected at bow and stern, in order to keep the model at an average heading of about 90deg (beam waves) (Bulian and Francescutto, 2013; Tzamtzis, 2004). In the simulations reported in Fig. 6, the model was free to drift laterally under the action of waves. However, in order to keep a heading of approximately 90deg, mimicking the effect of the manual control, rotations around the earth-fixed vertical axis were restrained through an artificial linear torque restoring spring having constant equal to $K_{spring} = 5.3{\cdot}10^8 N{\cdot}m/rad$. The moment generated by this spring has, therefore, components $\left(0, 0, -K_{spring}\psi\right)^T_{\Sigma}$ with respect to the earth-fixed reference system Σ, and acts as a proportional control. The introduction of this artificial spring leads to a yaw natural frequency, as measured from simulated yaw decays, of $0.0673 rad/s$, which is far enough from the roll natural frequency to reduce the risk of spurious couplings. The total simulation time was set to 900s, and roll motion was analysed in the final part of the time histories.

Results in Fig. 6 indicate a good agreement between experiments and simulations, with the agreement being better at lower rolling amplitudes. The simulation code is also able to reproduce the observed nonlinear effect of the bending of roll response curve to high frequencies. This is typical, both in regular (Francescutto and Contento, 1999b) and irregular (Bulian and Francescutto, 2011; Francescutto and Naito, 2004) waves, of ships having a hardening-type roll restoring, as in the present case (see Fig. 5).

Finally, the global dissipation level achieved after the tuning process has been quantified by usual 1-DOF roll damping coefficients coming from the analysis of simulated roll decays in calm water. The analysis has been carried out according to the methodology described by Bulian et al. (2009), and results of the roll decays analysis are reported in Table 3.

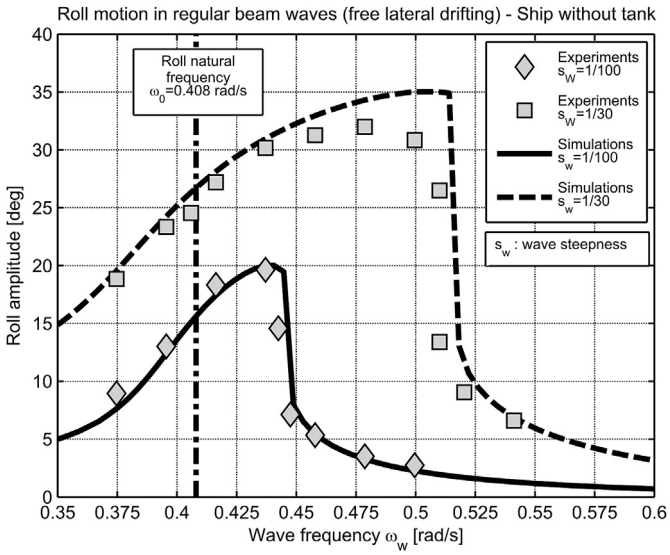

Fig. 6. Roll response in regular beam waves for ship without tank. Comparison between experiments and numerical simulations after the tuning process.

Table 3
Roll damping coefficients of the tuned ship motions model from analysis of simulated roll decays.

1-DOF mathematical model	$\ddot{\phi} + 2\mu\dot{\phi} + \beta\dot{\phi}\lvert\dot{\phi}\rvert + \delta\dot{\phi}^3 + \omega_0^2 r(\phi) = 0$ with $r(\phi) = \phi + \gamma_3\phi^3 + \gamma_5\phi^5 + \ldots$
Roll natural frequency	$\omega_0 = 0.408 rad/s$
Roll damping coefficients	$\mu = 0.00340 s^{-1} \Rightarrow \mu/\omega_0 = 0.833 \cdot 10^{-2}$ $\beta = 0.0994 rad^{-1}$ $\delta = 0.554 s \cdot rad^{-2} \Rightarrow \delta\omega_0 = 0.226$

3.3. Effect of tank length

A first series of simulations has been carried out in beam regular waves with the aim of assessing the effect of the tank length in mild sea conditions. To this end the three different tank lengths as specified in Table 2 have been considered, and the roll motion was simulated in regular beam waves of constant wave steepness $s_W = 1/100$ in a range of wave frequencies corresponding to the interval $[0.2\omega_0, 2.0\omega_0]$. For the considered steepness, numerical simulations and experimental results for the same vessel without the tank were available as reference (see Bulian and Francescutto, 2013; Tzamtzis, 2004; and Fig. 6).

In all simulations the model was free to drift laterally, and in order to keep a heading of approximately 90deg (beam waves coming from starboard), mimicking the effect of the manual control, rotations around the earth-fixed vertical axes were restrained through an artificial linear restoring spring with constant equal to $5.3 \cdot 10^8 N \cdot m/rad$, in line with what was done for the tuning of the 6-DOF code in section 3.2. All simulations have been carried out considering fresh water, in order to be relevant for possible experimental tests.

The total length of each simulation was set to 500s, with an initial ramp of 50s on the wave forcing. Considering that in all simulations the vessel starts from rest, a 2s pre-stabilization of the SPH solver was also performed before starting each simulation in order to reduce initial transient effects. The average roll amplitude was measured considering the final part of each simulation (time window corresponding to the final four full roll cycles or to the final 300s, whichever is minimum). Herein, the roll amplitude is conventionally defined as half of the difference between maximum and minimum roll within each cycle, in order to automatically remove the effect of asymmetric roll bias.

In SHIXDOF, a time step of 0.01s was used for tank lengths of 5 m and 10 m, while a reduced time step of 0.005s was necessary in order to guarantee stability of the coupled simulation for the tank length of 20 m. According to section 2.3.1 (see also Fig. 1), these are the time steps at which force data from the SPH solver are gathered. The integration time step used by the SPH solver within each ship motions simulation step was, instead, controlled by the Courant condition (11). Details of SPH simulations parameters are reported in Table 4. The selection of the number of particles was based on the idea of trying to keep approximately the same computational time among the three tank lengths, while still keeping a sufficient discretization. However, from the reported values, it is evident that the discretization is eventually finer for the shorter tanks. For the analysed ranges of frequencies and steepnesses, the maximum speed induced by ship motions at the bottom of the tank in absence of fluid in the tank is about 8 m/s. When applying (13), this leads to a minimum indicative limit for the speed of sound of 150 m/s, which is below the speed of sound of 200 m/s which has eventually been used in the present simulations.

Table 4
SPH simulation parameters.

Tank length [m]	5	10	20
Water density [kg/m^3]	1000	1000	1000
Kinematic viscosity [m^2/s]	10^{-6}	10^{-6}	10^{-6}
Number of fluid particles [-]	$1.1 \cdot 10^4$	$1.2 \cdot 10^4$	$1.3 \cdot 10^4$
Speed of sound [m/s]	200	200	200
Kernel characteristic length ratio $h/\Delta r$ [-]	3	3	3
Courant factor [-]	0.25	0.25	0.25

Results from the analysis of simulations are shown in Fig. 7, where the roll response curve without tank is compared with the roll response curve as obtained for the three simulated lengths of the tank.

In case of tank lengths 10 m and 20 m, the roll response curve in Fig. 7 shows the well-known double-peak shape (e.g., Field and Martin, 1976; Francescutto and Contento, 1999a; Kim et al., 2007; Lee and Vassalos, 1996; and discussion by Bell in van den Bosch and Vugts (1966)). The roll motion is strongly suppressed in the frequency region close to the roll natural frequency without tank (ω_0), but two side peaks appear at low and high frequency, and in these regions of wave frequencies the tank has a detrimental effect on roll motion. On the other hand, for the shortest tank, a different behaviour is observed, which indicates the reduced effectiveness of this tank as an anti-rolling device. The roll response for the tank having a length of 5 m becomes essentially single-peak, with the main peak observed for frequencies close to, but slightly smaller than, ω_0. Together with the presence of the main peak for the shortest tank, a hump in the response curve can still be noticed in the low frequency region. Such hump looks like a reminiscence of the double-peak behaviour observed for the two longer tanks, or, in a way, of the double-peak behaviour which could reasonably be expected if the shortest tank were actually effective similarly to the longer tanks. It is also interesting to note the tendency for the main peak to be skewed towards the high frequency region, in accordance with the hardening behaviour of the roll righting moment in calm water (see Fig. 5). As a result, the roll response curve for the considered wave steepness seems to undergo a transition as the tank length increases: starting from a single-peak behaviour without tank, the double-peak behaviour is achieved only for tanks having sufficient longitudinal extent, while an intermediate behaviour is noticed for the case of short tanks. As a result, the shortest tank has a more limited effect as anti-rolling device. It is interesting to note that the longer the tank, the larger it is its effectiveness in the wave frequency region close to the roll natural frequency. However, as it is known, the by-product of using passive free surface tanks is an increase of the rolling motion at high frequency and in the region of low frequencies, which is confirmed in the present simulations. The increase of rolling motion at high frequency is largest for the longest tank. On the other hand, the amplitude of the peak at low frequency is approximately the same for the

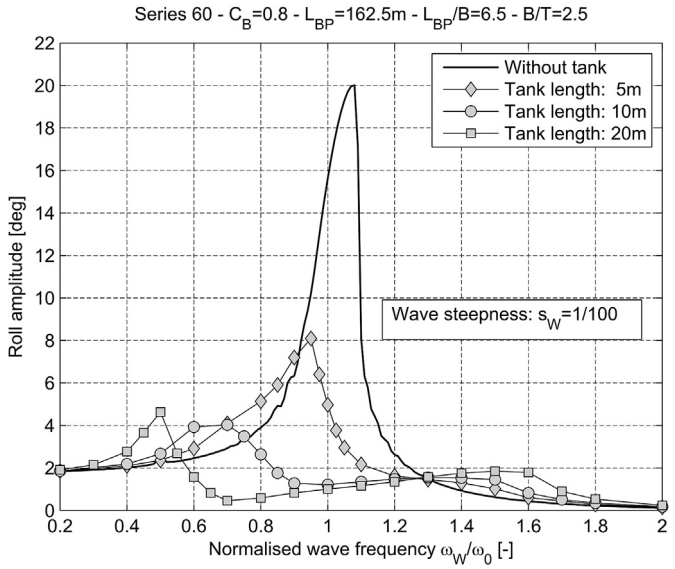

Fig. 7. Roll response in regular beam waves. Vessel without tank and vessel with tanks of different length.

two longer tanks. The longest tank leads to a secondary peak at a lowest frequency and the width of the peak is smaller compared to the tank of intermediate length. The frequency of maximum suppression, i.e. the frequency with the lowest roll motion, shifts toward lower frequencies as the tank length increases.

Looking at Fig. 7 for the vessel without tank, some oscillations are visible in the reported roll response curve, mostly around $\omega_W/\omega_0 = 0.8$ and $\omega_W/\omega_0 = 1.1$. Such oscillations are due to transient behaviours which do not completely die out for the considered simulation time (500s). Such transient behaviours, then, slightly influence the determination of the representative roll amplitude as determined from the simulated roll time histories. However the overall effect is sufficiently small for practical purposes to be considered acceptable. It is noted that such effects are not visible in Fig. 6 because the corresponding simulations have been run for a longer time (900s vs 500s), thus achieving a better steady state, and because part of the frequency region interested by these effects is outside the frequency range reported in Fig. 6. Some transient behaviour is also still visible at the end of some time histories from simulations with the shortest tank in the region of wave frequencies close to the peak of the response curve. Example roll time histories corresponding to the case $\omega_W/\omega_0 = 0.9$ are shown in Fig. 8.

It is now interesting to look at the obtained results in view of the stabilizer capacity η_{tank} as reported in Table 2. However, since η_{tank} represents a nominal limiting effective wave slope value, a comparison with the results in Fig. 7 requires the estimation of the effective wave slope coefficient r_W. The effective wave slope coefficient for the considered vessel has therefore been estimated according to the methodology described by Bulian and Francescutto (2009), considering the fluid in the tank as "frozen" and a reference frequency of 0.408 rad/s. Results from the calculations are reported in Table 5, where the effective wave slope has been calculated also for the vessel without tank. It can be seen that all the calculated nominal critical wave steepnesses $s_{W,crit,nom}$ are above the steepness 1/100 used in Fig. 7, and therefore all the three considered tank lengths would be nominally effective in the tested conditions if using the stabilizer capacity η_{tank} as a reference. However, according to the simulations, the tank with length of 5 m has already started losing efficiency with the considered steepness of 1/100, this indicating a critical wave steepness from simulations which is somewhat lower than 1/100. At the same time, $s_{W,crit,nom}$ in Table 5 for the tank length of 5 m is 1/84. Therefore, according to the calculations carried out, the critical wave steepness determined by means of the stabilizer capacity parameter as defined by Beck et al. (1989), combined with the determination of the effective wave slope coefficient according to Bulian and Francescutto (2009), overestimates the limiting wave steepness which can be obtained from the direct simulations in the considered case, although the two steepnesses are similar. This overestimation could be due, on the one hand, to the approximate nature of the linearized approach used in the method by Bulian and Francescutto (2009) for the determination of the

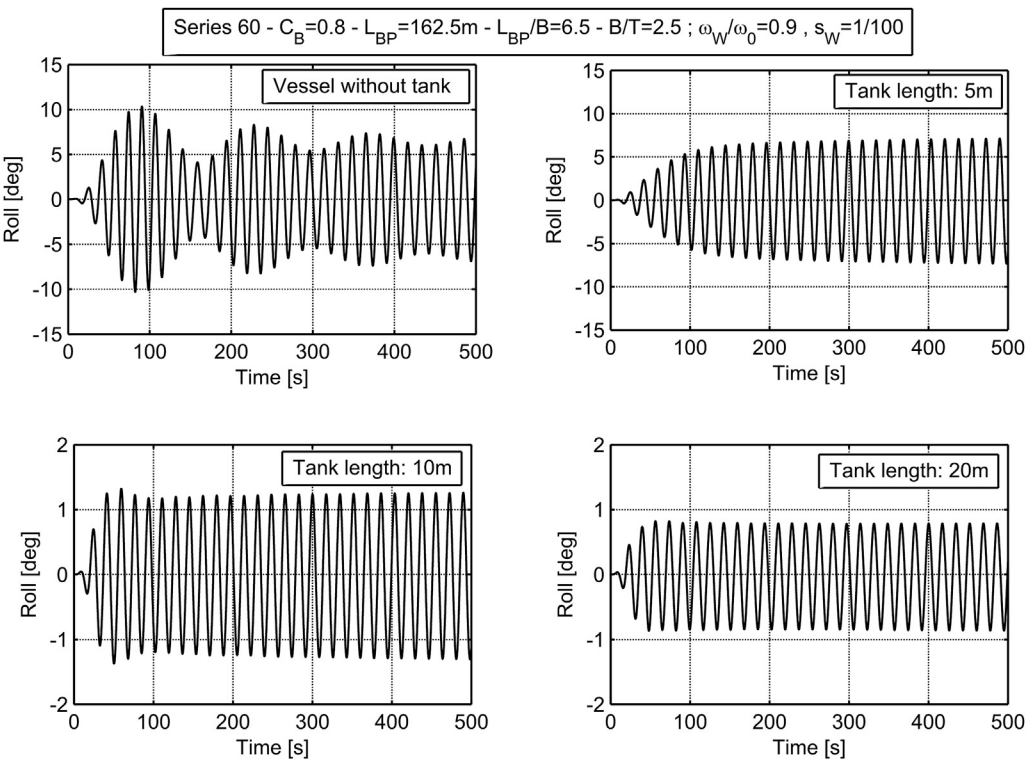

Fig. 8. Example roll time histories in regular beam waves with $\omega_W/\omega_0 = 0.9$ and $s_W = 1/100$. Vessel without tank and vessel with tanks of different length.

Table 5
Effective wave slope coefficient and nominal critical wave slope/steepness.

Tank length	[m]	Without tank	5	10	20
Ship draught	[m]	10.00	10.04	10.08	10.15
Stabilizer capacity η_{tank}	[−]	–	0.0255	0.0526	0.1111
Effective wave slope coefficient r_W	[−]	0.69	0.68	0.67	0.66
Nominal critical wave slope $\alpha_{crit,nom} = \frac{\eta_{tank}}{r_W}$	[−]	–	0.0375	0.0785	0.1683
Nominal critical wave steepness $s_{W,crit,nom} = \frac{\alpha_{crit,nom}}{\pi}$	[−]	–	0.0119 1/84	0.0250 1/40	0.0536 1/19

effective wave slope coefficient, while the actual problem is, instead, nonlinear. On the other hand, the overestimation could also be due to the assumption, used in the determination of η_{tank}, that the tank is able to generate a maximum moment associated with the fluid all placed at the extreme side of the tank, and this is a convenient, but optimistic, idealization.

3.4. Effect of wave steepness

In the previous section, the behaviour of the coupled system has been assessed for a series of different tank lengths. Scope of this section is to investigate the effect of increasing the wave forcing, i.e. the wave steepness. Roll motion is indeed known to behave nonlinearly as the wave forcing increases. This is due to the effects of, mainly, nonlinear roll damping and nonlinear roll restoring (e.g. Bulian and Francescutto, 2011, 2013; Bulian et al., 2012; Cardo et al., 1981, 1982; Francescutto and Contento, 1999b; Francescutto and Naito, 2004; Hashimoto et al., 2012; Himeno, 1981; Holden and Fossen, 2012; Kawahara et al., 2009; de Kat and Paulling, 1989; Matusiak, 2007; el Moctar et al., 2012; Neves et al., 2009; Sadat-Hosseini et al., 2010; Sinibaldi and Bulian, 2014; Tzamtzis, 2004). In addition, the sloshing flow inside the tank is also expected to behave nonlinearly as the motions (particularly roll, sway and yaw) increase as a consequence of the increase in the wave forcing. In the condition under investigation, this is particularly expected also because of the shallow water level in the tank (see Table 2). Since the tools used in the co-simulation approach are able, in principle, to address such nonlinear effects, the global co-simulation approach is expected to be able to handle such nonlinear effects considering the two-way coupling between the two sub-systems.

To investigate the mentioned expected nonlinear phenomena, the configuration with a tank length of 10 m has been chosen. In addition to the wave steepness 1/100 investigated in the previous section, herein motions are simulated for four additional wave steepnesses, namely: 1/80, 1/67, 1/57 and 1/50. The set of simulation frequencies for each wave steepness has been adapted in order to give a clear representation of the roll response curve, particularly close to the peak regions. In order to allow assessing the effectiveness of the tank as an anti-rolling device, simulations have been carried out considering the vessel with and without the tank. The simulation parameters, as well as the definition of rolling amplitude obtained from simulated time histories, are the same as those used in the previous section. Results of simulations are shown in terms of dimensional rolling amplitude in Fig. 9. In order to more clearly highlight nonlinear effects, Fig. 10 reports roll amplitude data in normalised form using, as normalising factor, the maximum wave slope $k_W a_W = \pi s_w$.

From the results reported in Figs. 9 and 10, it can be noticed that the vessel without the tank follows the classical well-known nonlinear behaviour in regular beam waves, with a peak roll response which increases less-than-linearly as a function of the wave steepness, and a bending of the response curve towards the region of high frequencies. The less-than-linear increase of the roll peak is particularly well highlighted when reporting data in normalised form in Fig. 10, from which it can be clearly noticed the reduction of the normalised peak as the wave steepness increases. The bending of the response curve is in accordance with the hardening behaviour of the roll righting moment in calm water (see Fig. 5). A small ultra-harmonic resonance (Cardo et al., 1981) is also visible at $\omega_W/\omega_0 \approx 0.5$ as a small peak in the response curve. In such condition, in addition to the harmonic component at the encounter wave frequency, roll motion is characterised by a significant harmonic component at twice the encounter wave frequency, which is in turn close to the roll natural frequency ω_0.

Looking at the behaviour of the roll response of the vessel with the tank partially filled with fluid, it can be noticed that the effect of the tank, as an anti-rolling device, is very significant in case of the lower forcing steepnesses, up to $s_W = 1/67$. On the other hand, the roll response for $s_W = 1/50$ is much different and it is, essentially, single-peak with a small hump in the low frequency region. Such type of response looks qualitatively similar to the one observed for $s_W = 1/100$ and a tank length of 5 m. The forcing case with $s_W = 1/57$ is characterised by an intermediate, transitional character. Such transitional character manifests also in time domain, as long transients before stationarity. This is a similar situation as the one identified when considering different tank lengths. Looking, in particular, at the results reported as in Fig. 10 it can be seen that the normalised roll response of the vessel with the tank has a more diversified behaviour compared to what can be observed for the vessel without tank. In fact, in the region of wave frequencies close to the high-frequency peak, the roll response of the vessel with the tank tends to behave, overall, less-than-linearly. Conversely, in the lower frequency region the normalised roll response for the vessel with the tank tends to increase as the wave steepness increases, indicating a tendency towards a more-than-linear dependence of the roll response on the wave steepness. This behaviour indicates that the roll suppression effect of the tank, as an anti-rolling device, tends to decrease as the wave forcing increases. This behaviour is qualitatively in line with the indications given by Beck et al. (1989), that anti-rolling tanks tend to decrease their roll suppression effect in irregular sea if the significant wave height is too high.

Furthermore, it is also interesting to report that the small ultra-harmonic response which was observed in the simulations without

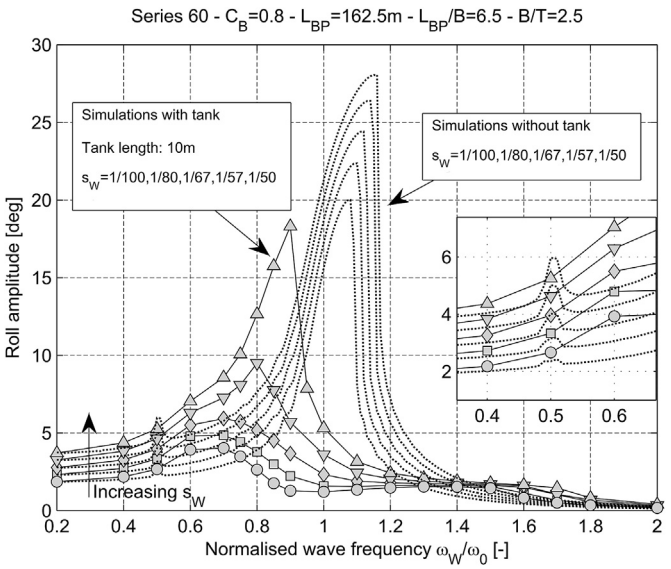

Fig. 9. Roll response in regular beam waves. Vessel without tank and vessel with tank, for different forcing wave steepnesses.

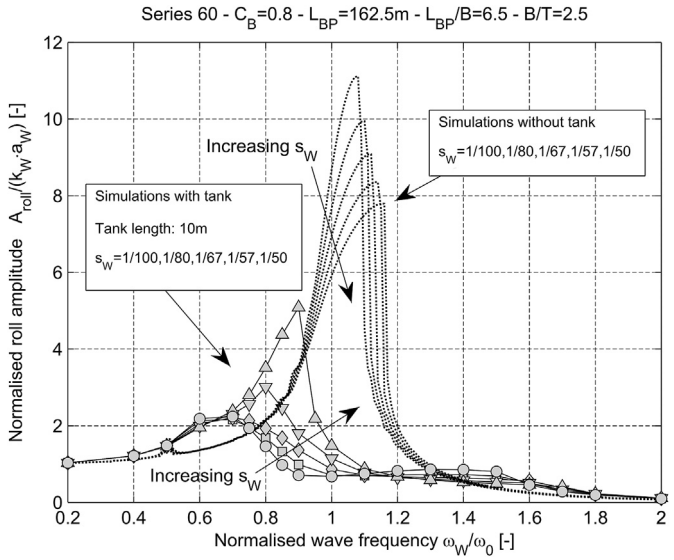

Fig. 10. Normalised roll response in regular beam waves. Vessel without tank and vessel with tank, for different forcing wave steepnesses.

tank has not been observed in simulations carried out with the tank. This could mean that the tank was able to suppress the inception of the small ultra-harmonic resonance. It is however also reasonable to assume that, if the phenomenon is still present, the fitting of the tank could have shifted its occurrence to a different frequency region, and that the frequency range and frequency discretization used for simulations with the tank are not appropriate to disclose it.

Similarly to what has been observed in the previous section, some oscillations are visible in the roll response curve for the vessel without tank, particularly in the region close to $\omega_W/\omega_0 = 0.8$, due to the transients which are still visible at the end of the simulation time (500s). The occurrence of quite long transients can also be observed in some simulations carried out with the tank, particularly around the peak of the response curve for steepnesses 1/57 and 1/50. Example roll time histories corresponding to the case $\omega_W/\omega_0 = 0.8$ are shown in Fig. 11.

From the results in Figs. 9 and 10 it can therefore be said that, according to the simulations, the stabilizer loses efficiency for a wave steepness between 1/67 and 1/57. According to Table 5 the critical wave steepness for this tank length is, instead, 1/40. Similarly to what has been observed in the previous section for a tank length of 5 m, also for the tank length of 10 m the approach based on the use of the stabilizer capacity η_{tank} overestimates the critical wave steepness for the reduction of tank effectiveness compared to what is determined from simulations.

As a support to the results of the simulations reported in Figs. 9 and 10, a sensitivity assessment with respect to the particle discretization has been carried out by means of two additional sets of simulations with increased number of particles. The number of particles was increased by a factor of approximately five and ten, leading to approximately $6.3{\cdot}10^4$ and $1.2{\cdot}10^5$ particles, respectively. For reasons associated with the stability of the coupling algorithm, it was found necessary to decrease, in both cases, the time step in SHIXDOF to 0.005s, i.e. half of the time step used for the standard simulations with $1.2{\cdot}10^4$ particles. However, in case of such a large number of particles, the SPH solver represents the heavier part of the simulation, and therefore the reduction of the time step in the ship motions solver has little effect on the global computational time. It is also worth reporting that a reduction of the time step in SHIXDOF from 0.010s to 0.005s when the number of particles is $1.2{\cdot}10^4$ has a negligible effect on the results. Simulations have been performed for the frequency ratio $\omega_W/\omega_0 = 0.9$ and wave steepnesses 1/100, 1/80, 1/57 and 1/50. The frequency has been chosen in order to capture both the region of strong roll suppression in case of the smallest forcing steepness and the region of peak of the roll response curve when considering the largest forcing steepness (see Figs. 9 and 10). The four steepnesses have been selected in order to cover both the regime of small rolling amplitudes and the regime of large rolling amplitudes. Furthermore, the selected conditions also allow to pass through the region of transition from where the tank is effective to where the tank starts becoming not effective as anti-rolling device. Resulting roll amplitudes

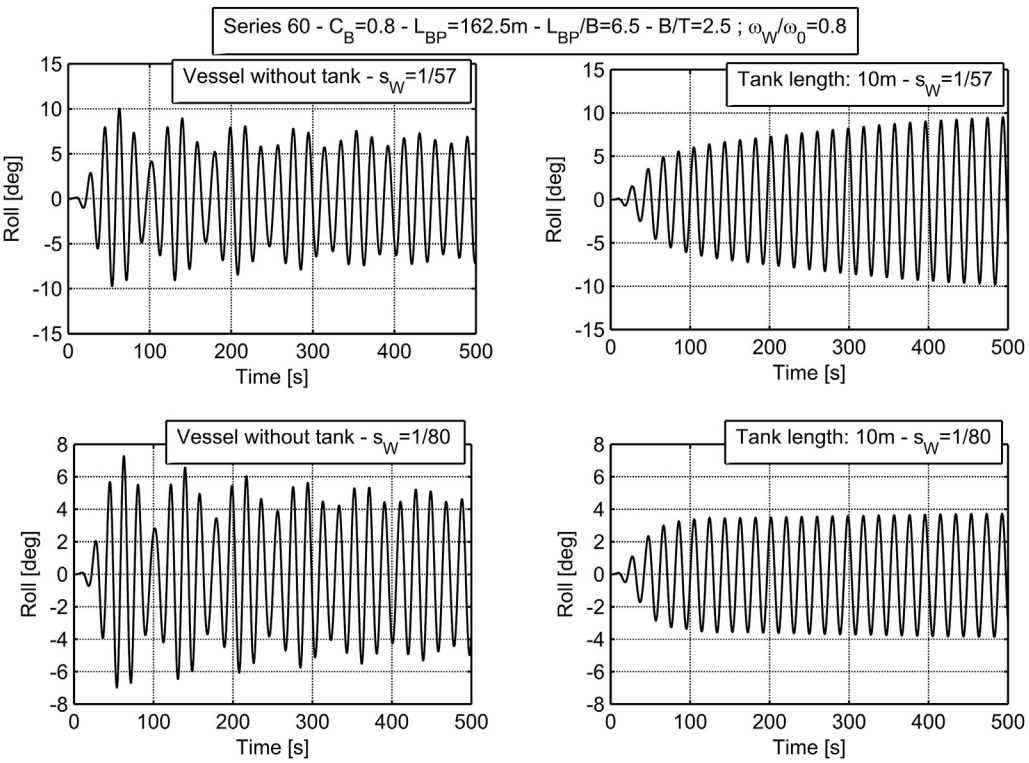

Fig. 11. Example roll time histories in regular beam waves with $\omega_W/\omega_0 = 0.8$ and different wave steepnesses. Vessel without tank and vessel with tank having length of 10 m.

are compared in Fig. 12. It can be noticed that results with $6.3{\cdot}10^4$ and $1.2{\cdot}10^5$ particles basically coincide, indicating that the corresponding data can be considered as a reference. The comparison between results at different levels of discretization shows that, in general, for the considered case and conditions, higher resolution simulations tend to provide smaller rolling amplitudes compared to simulations with a smaller number of particles. However, it can be noticed that, although some differences are visible, such differences are small. Such level of discrepancy could likely be considered as an acceptable trade-off when considering that each single simulation using the reference number of particles ($1.2{\cdot}10^4$) runs, on average, in less than 4 h, while the computational time increases to about 16 h ($6.3{\cdot}10^4$ particles) and 35 h ($1.2{\cdot}10^5$ particles) for the higher resolution simulations.

An analysis of the force exerted by the fluid in the tank on the vessel has also been carried out. In particular, the component F_y of the force along the ship-fixed transversal axis, i.e. the lateral force, has been considered. In order to eliminate the high frequency noise coming from the SPH solver, the force signals have been mildly low-passed, and the resulting filtered signal $F_{y,filt}$ has been used in the analysis. The forces have been analysed in the final part of each simulation, considering the last four (three for the lowest simulated frequency) oscillation periods. Example time histories of the lateral force F_y and $F_{y,filt}$ are shown in Fig. 13 for a set of four different wave frequencies in case of wave steepness 1/80. It can be noticed that, due to nonlinear effects, the time histories of the force significantly depart from the sinusoidal behaviour which would instead be observed in the framework of a linear approach. For all the simulated cases, two quantities have been determined from the time histories of $F_{y,filt}$: the maximum absolute value and the standard deviation. Results from this analysis are shown in Fig. 14, where both the maximum absolute value as well as the standard deviation of $F_{y,filt}$ tend to show two peaks, corresponding to the low-frequency and high-frequency peaks of the roll response curve. The behaviour of the standard deviation is smoother and more regular compared to that of the maximum absolute value. This is a consequence of the fact that the standard deviation is much less influenced by localised (in time) peak phenomena, which are instead governing the maximum absolute value in certain conditions in the high frequency region. It can also be noticed that the previously discussed loss of effectiveness of the tank, with the associated increase of roll motion (see Figs. 9 and 10), leads to a corresponding increase of the lateral force exerted on the vessel, i.e., in real situations, on the tank structure.

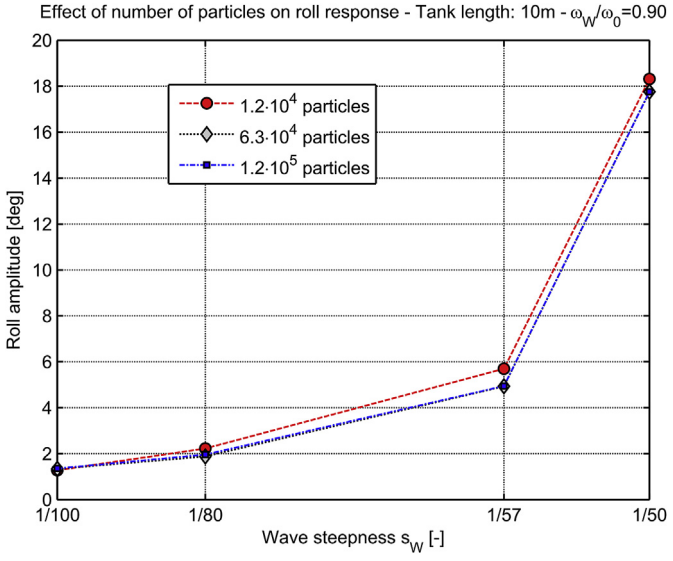

Fig. 12. Effect of number of particles on roll response. Tank length: 10 m. Frequency ratio: $\omega_W/\omega_0 = 0.9$.

Finally, Fig. 15 shows the simulated fluid behaviour inside the tank, together with the correspondingly computed pressure field, for a set of example cases. The reported cases correspond to frequency ratios ω/ω_0 equal to 0.7, 0.8, 0.9 and 1.0, and two forcing wave steepnesses, namely 1/80 and 1/50. The reported snapshots are taken at four representative time instants within the last available roll cycle, corresponding to: minimum roll, up-zero-crossing for roll, maximum roll and down-zero-crossing for roll. In this way the set of snapshots can give a quite good idea of the overall fluid behaviour in a single roll cycle. When looking at the reported snapshots it shall be borne in mind that they represent two-dimensional projections of an actually three-dimensional field measured at discrete points corresponding to the positions of particles.

3.5. Simulation performance

As it has been previously discussed, for real applications the performance aspect becomes critical, and therefore it should be analysed. To carry out the performance test, SHIXDOF was run on a workstation with two CPUs Intel Xeon Processor E5-2687 W (16 cores in total) at the University of Trieste, Italy, while AQUAgpusph was run on a GPU NVidia GTX Titan (GK110) at the Technical University of Madrid (UPM), Spain. It shall however be noted that SHIXDOF is not explicitly parallelised, and therefore similar performances can be expected also when using a more limited number of cores.

In Fig. 16 the time consumed to perform each simulation, considering the tank of 5 m and the wave steepness $s_W = 1/100$, are depicted. A separation is also highlighted between two series of simulations which were carried out one after the other. Simulations within each set were carried out in sequential increasing frequency order. As it can be appreciated, each simulation requires less than 4 h to be carried out. In the same figure, the time required for AQUAgpusph and for SHIXDOF plus network communication are separately reported, as measured from the server side (see Fig. 2). In addition, the time associated with only SHIXDOF is also reported, as estimated from separate simulations without tank. Such time is not very variable and corresponds to about 0.3 h. Regarding AQUAgpusph, its performance may be affected by the flow dynamics, and more precisely by the number of neighbours per particle, showing a dependency on the wave frequency. Finally, the time required by the network communication is very variable, and, in certain cases, it became the most time consuming part of the simulation. It must be remarked however, that, at the present stage of development, for debugging purposes, some redundant information is exchanged between the tools, and this inevitably increases the network communication time compared to an optimized implementation. It should also be noted that a local installation on the same hardware can reduce the network communication time to a negligible level.

4. Conclusions

With the aim of dealing with nonlinear ship motions and nonlinear sloshing in a consistent two-way coupled way, this paper has presented a simulation approach where a blended (hybrid) nonlinear 6-DOF ship motions simulation code (SHIXDOF) has been coupled with a nonlinear WC-SPH solver (AQUAgpusph) intended to address the flow in the internal tank. The ship motions code allows to simulate nonlinear ship motions and manoeuvring in wind and waves using a system-based modelling. The SPH solver allows to deal with three-dimensional, possibly violent, sloshing, considering arbitrary tank motions.

The coupling has been carried out using a co-simulation strategy which is suitable for loosely coupled systems, as the in the case herein. Such co-simulation strategy has been developed with a GRID computing paradigm in mind. In the developed co-simulation strategy, SHIXDOF acts as a client, while AQUAgpusph acts as a server. The two subsystems exchange information in terms of force and displacements, and the communication between the two subsystems occurs through a network connection, using TCP/IP protocol.

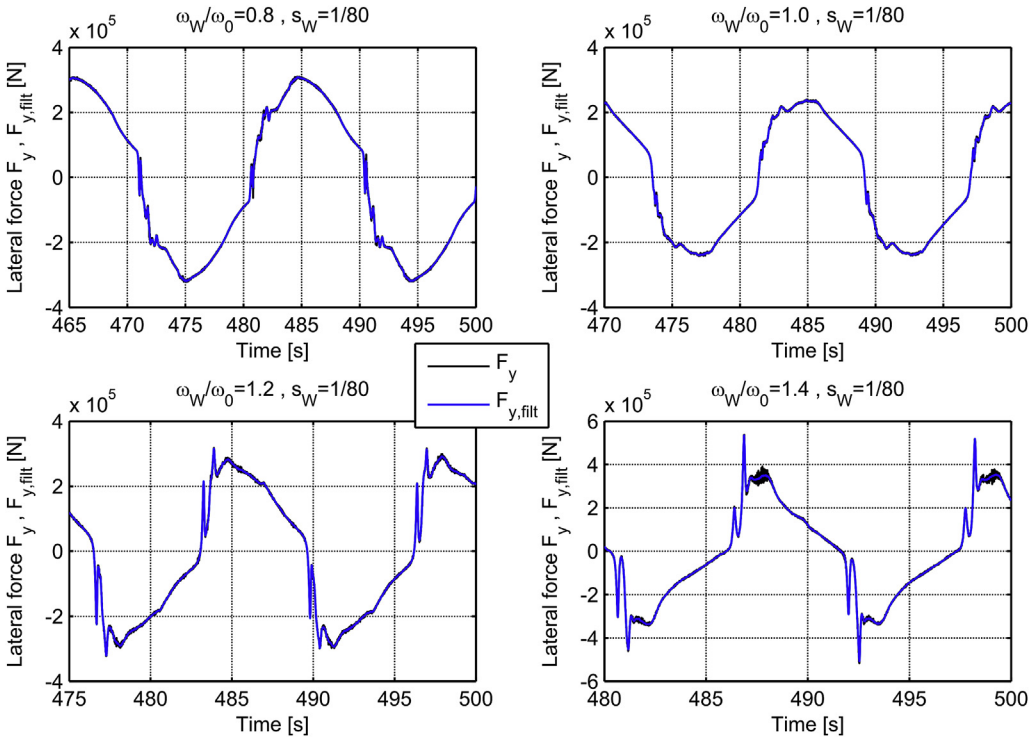

Fig. 13. Example time histories of lateral force F_y and filtered lateral force $F_{y,filt}$. Tank length: 10 m. Wave steepness $s_W = 1/80$.

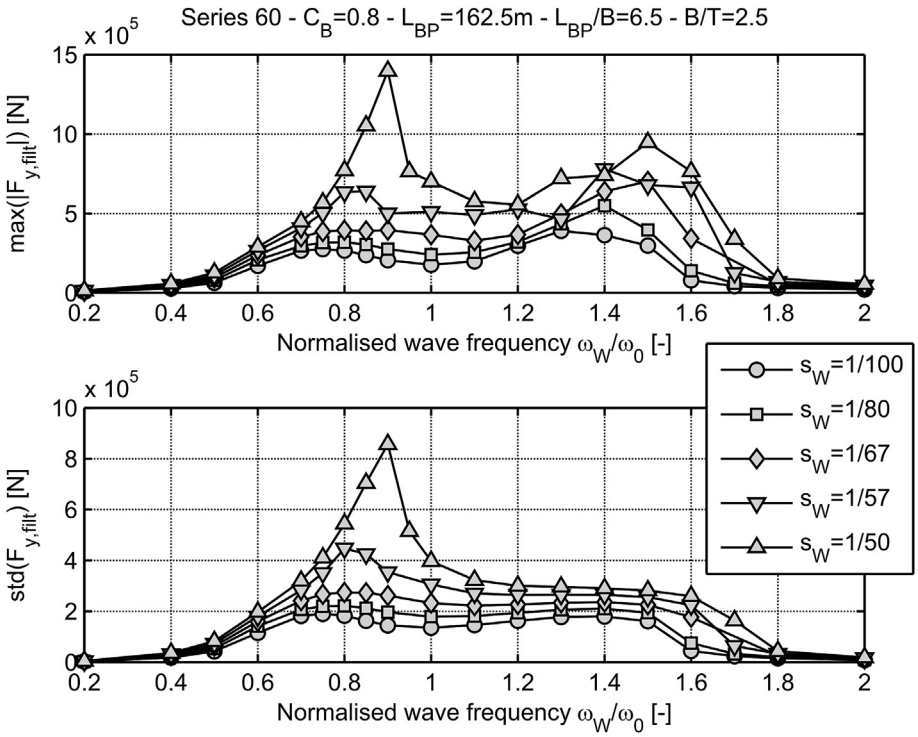

Fig. 14. Maximum absolute value (top) and standard deviation (bottom) of the filtered lateral force $F_{y,filt}$. Tank length: 10 m.

An application of the developed tool has been carried out for a Series 60 hull equipped with a partially filled box shaped tank, and three different longitudinal extents of the tank have been considered. The used geometry has been selected since it is well known and freely available. In the application, the considered tanks have been intended to act as anti-rolling devices, and the fluid depth was selected accordingly, by tuning of the first linear transversal sloshing mode to the roll natural frequency of the vessel. This eventually led to a small fluid depth to tank width ratio, and therefore sloshing was characterised by a shallow water fluid regime.

Two different sets of simulations have been carried out in regular beam waves. One set of simulations was intended to address the effect of the tank dimensions in the (almost) linear range. Accordingly, the three different tank lengths were tested considering a single constant small wave steepness. Another set of simulations was intended to address nonlinear effects associated with large forcing, with consequent large

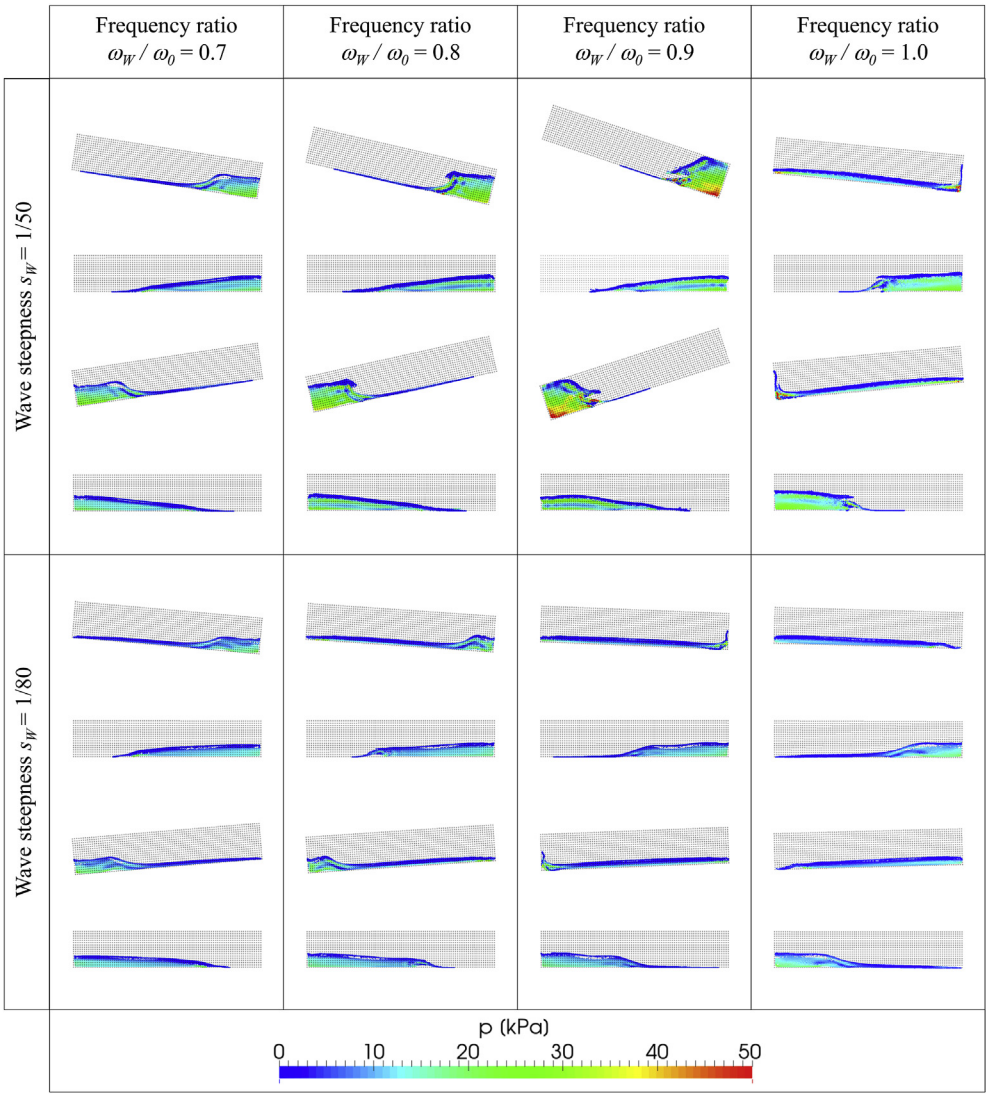

Fig. 15. Representative snapshots of pressure field of fluid inside the tank.

motions and violent sloshing. To this end, a single tank length (the intermediate one) was selected, and different increasing wave steepnesses were used in the simulations. Before carrying out coupled simulations, the 6-DOF ship motions code was tuned, in terms of roll dissipation, using available experimental data for the vessel without tank.

Results from simulations for the two longer tested tank lengths have led to the classical double-peak behaviour for the roll response curve, with suppression of roll motion close to the natural frequency, and increase of roll at low and high frequency. However the shortest tank length has proved to be much less effective as an anti-rolling device for the tested wave steepness, leading to a basically single-peak roll response, with some reminiscence of the double-peak behaviour. When testing the intermediate tank length with variable forcing steepness, a similar behaviour was observed. Indeed, the roll response remained double-peak for the lower forcing steepnesses. However, a transition towards a single-peak roll response was observed when increasing the wave steepness, with a consequent significant reduction of the tank effectiveness as an anti-rolling device. The type of used simulation tools allowed to observe the typical nonlinear phenomenon of bending of the roll response curve for the vessel with and without tank. The nonlinear dependence of the roll amplitude on the wave steepness was also observed in the simulations. In addition, in case of vessel without tank, a small ultra-harmonic roll response was observed at wave frequencies close to half the roll natural frequency. The same type of response was not observed when the vessel was fitted with the tanks. It is however not evident whether this response was suppressed by the tank presence, or whether this peculiar response was simply missed due the considered frequency range and the rougher frequency discretization compared to that used in case of vessel without tank.

An additional application has been carried out for validation purposes considering roll and also heave motion with and without a partially filled tank for a 200kDWT tanker, for which data were available in literature. Simulations from the coupled numerical tool have shown an overall satisfactory agreement with experimental data, both with and without fluid in the tank. However, some remarks regarding the original experimental setup and results have been reported, which arose during the setting up of the simulation campaign in this study. It is interesting to note that, although such case was used in the past for other, different, validation studies and papers, we could not find such notes in the literature.

Compared to some of the already existing alternatives available in literature, the presented approach has the important characteristics of being fully nonlinear, and this makes it able to deal with the assessment of ship safety in severe environmental conditions. In addition, although the developed approach has been tested herein at zero forward speed in beam regular waves with a box-shaped tank, the software architecture is more flexible. Indeed, the 6-DOF code allows simulating ship motions in case of the vessel manoeuvring in regular/irregular waves, and constant/

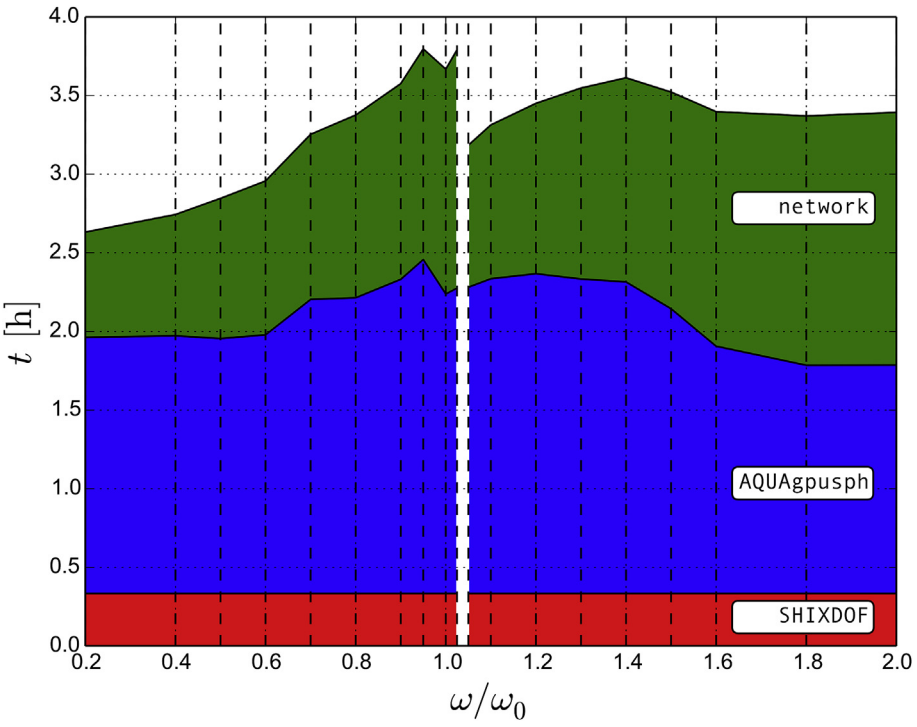

Fig. 16. Analysis of simulation time. Tank length equal to 5 m and wave steepness equal to 1/100.

gusty wind, considering the coupling with the tank. Furthermore, the SPH solver allows taking into account more complex tank geometries (e.g. non box-shaped tanks, presence of baffles and obstructions, etc.). As a result, in addition to representing a valuable tool for research purposes, there are potentialities for this approach to be used for more practical engineering applications. Example practical applications concern the analysis of efficiency of passive anti rolling tanks considering also large amplitude ship motions and specific nonlinear phenomena (e.g. parametric roll), the analysis of dynamic free surface effects on FPSOs and LNG carriers, the transferring of pressure loads to structural models, etc.

The implemented co-simulation strategy is very flexible and scalable. The tools can indeed run on different hardware and software environments, and in different computing facilities. Also, the co-simulation strategy allows, in principle, simulating ship motions with an arbitrary number of tanks, and the simulation of the fluid flow within each tank can possibly be carried out on different hardware. The implemented co-simulation strategy based on TCP/IP communication is also efficient. This efficiency comes from the fact that the amount of information transferred between both codes is, in general, small. This is also a consequence of the fact that the communication task is executed every few hundreds SPH time-steps, since time stepping in the SPH solver is typically much smaller than the time stepping used in the ship motions solver.

In addition, the developed approach seems also to be practical in terms of computational time. Indeed, each single simulation reported in this study required about 4 h of computational time, leading to the possibility of creating a roll response curve for a single steepness in about four days.

Considering the generality of the approach, a significant amount of future developments can be foreseen, dealing with, e.g., the following topics: further validation with experimental data, simulations with more complex tank geometries (e.g. tanks with baffles), ship motion predictions in presence of multiple tanks, simulations considering the vessel self-propelled and free running in wind and waves, modification of the SPH solver to work in the non-inertial ship-fixed reference system, application of the methodology in cluster architectures, optimization of SPH parameters for speeding up the calculations.

Acknowledgements

The research leading to these results has received funding from the Spanish Ministry for Economy and Competitiveness under grants TRA2013-41096-P (“Optimización del transporte de gas licuado en buques lng mediante estudios sobre interacción fluido-estructura”) and ENE2014-59194-C2-2-R (“X-Sheaks: campaña experimental y validación”). The authors are grateful to NVidia for the donated GTX-Titan computational device, which has allowed to carry out the simulations presented in this work. The authors would like to thank Dr. J. de Kat (ABS, Denmark), Prof. A. Papanikoalou (formerly NTUA, Greece - presently HSVA, Germany) and Prof. T. Santos (CENTEC, Portugal) for sharing information regarding the 200kDWT tanker test case. The authors would also like to thank Prof. Antonio Souto-Iglesias (UPM, Spain) for the continuous interesting and productive discussions and suggestions during the preparation of this paper.

Appendix

In the main text, an application has been thoroughly reported concerning a Series 60 hull with and without a partially filled tank, and simulations have been compared with experimental data in the case of the vessel without fluid in the tank. In this Appendix comparisons are provided between simulations and a set of available experimental data from de Kat (2000) for a 200kDWT tanker equipped with a free surface tank, which was tested at MARIN at 1:82.5 scale. The same vessel was also used in an ITTC benchmark (Papanikolaou and Spanos, 2004). The same simulation methodology as

the one detailed in the main text is used also in this Appendix, and therefore the approach is described more concisely.

Experimental data used herein refer to the case of the tanker without fluid in the tank, and to the case indicated as "resonant sloshing" by de Kat (2000). Experimental tests have been carried out in beam regular waves, with the model softly restrained. Data have been reported by de Kat (2000) for roll motion and for heave motion. The heave motion was measured at a point positioned at the centreplane, 49.5 m forward of the mid perpendicular, and 33.5 m above the baseline (full scale quantities). The main characteristics of the 200kDWT tanker without fluid in the tank are reported in Table A1. A front view of hull sections and tanks geometry is shown in Figure A1 and a side view of the centreplane is shown in Figure A2.

It is noted here that the dry roll radius of gyration of the vessel, as reported in Table A1, has been obtained by tuning of the roll response curve without tank on the availadle experimental data. In fact, at the beginning of the analysis, the tuning of the dry roll radius of gyration was based on the available experimental roll decay as reported by de Kat (2000). This led to a dry roll radius of gyration of $0.266B$, corresponding to a natural roll frequency of $0.639 rad/s$. Such setup was matching the available roll decay, but it was clearly incompatible with the available experimental data regarding roll motion, since, as it will be shown later in this section, the peak of the experimental roll response reported by de Kat (2000) is at a significantly lower frequency. Considering the large metacentric height of the vessel which leads to an almost linear restoring for a wide range of heeling angles, such significant shifting of the resonance peak could not be reasonably associated to nonlinear phenomena. In absence of further information, it was therefore decided to re-tune the dry roll radius of gyration using the experimental roll motion data in beam waves as reported by de Kat (2000). It is also noted here that de Kat (2000) reports $\overline{KG} = 10m$ corresponding to $\overline{GM} = 9.5m$, which would correspond to $\overline{KM} = 19.5m$. However, the value of $\overline{KM}$ corresponding to the three dimensional geometry reproduced herein from the bodyplan reported by de Kat (2000) was found to be 19.85 m, as reported in Table A1. After thorough checking, it was not possible to identify the source of the discrepancy, and it has therefore been decided to perform the simulations by fixing the value of $\overline{GM}$ for the vessel without the tank at the reported nominal value of 9.5 m, and to determine the value of $\overline{KG} = 10.35m$ as a consequence of the $\overline{KM}$ as obtained from the hull geometry.

According to de Kat (2000), the tank is positioned amidships, with a length of 82.5 m and a width of 31.76 m. The bottom of the tank is positioned 5.2 m from the ship bottom. Since the total height of the tank was not reported, a value of 23 m has been assumed by looking at the sketches reported by de Kat (2000). The depth of fluid in the tank is 4 m, corresponding to a first natural frequency for transversal sloshing of 0.604 rad/s. The increase of draught associate with the loading of the fluid is 0.777 m with a negligible trim, and the ratio between the mass of the tank and the mass of the vessel is 5.3%.

Table A.1
Data for the 200kDWT tanker without fluid in the tank. Full scale.

Length between perpendiculars - L_{BP}	[m]	310.2	Height of transversal metacentre above baseline – $\overline{KM}$	[m]	19.85
Breadth – B	[m]	47.2	Transversal metacentric height – $\overline{GM}$	[m]	9.5
Draught – T	[m]	16.0	Height of centre of gravity above baseline – $\overline{KG}$	[m]	10.35
Height of deck from baseline – H_{deck}	[m]	26.07	Roll natural frequency - ω_0	[rad/s]	0.607
Hull volume – ∇	[m^3]	197674	Dry roll radius of inertia w.r.t. CoG – $R_{xx,G}$	[m]	13.45
Waterplane area – A_{wp}	[m^2]	13451	Assumed dry pitch radius of inertia w.r.t. CoG – $R_{yy,G}$	[m]	77.6
Block coefficient – C_B	[−]	0.84	Assumed dry yaw radius of inertia w.r.t. CoG – $R_{zz,G}$	[m]	77.6
Coordinate of mid perpendicular – x_{MP}	[m]	155.1	$R_{xx,G}/B$	[−]	0.285
Length-breadth ratio – L_{BP}/B	[−]	6.57	$R_{yy,G}/L_{BP}$	[−]	0.250
Breadth-draught ratio – B/T	[−]	2.95	$R_{zz,G}/L_{BP}$	[−]	0.250

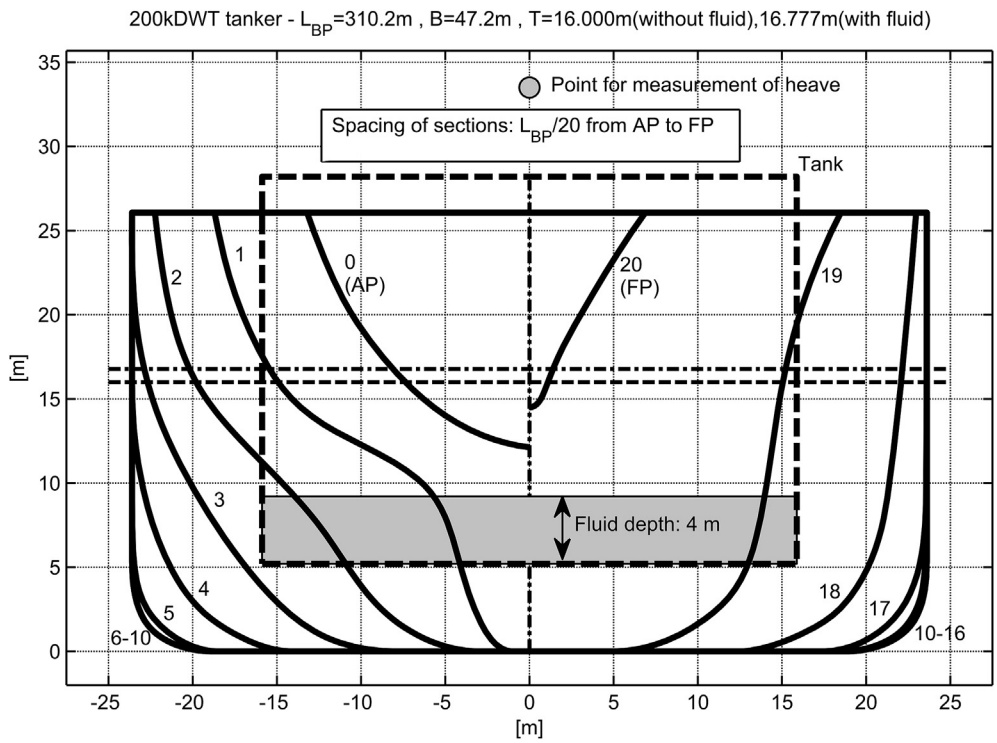

Fig. A.1. Front view of hull sections and tank geometry. 200kDWT tanker.

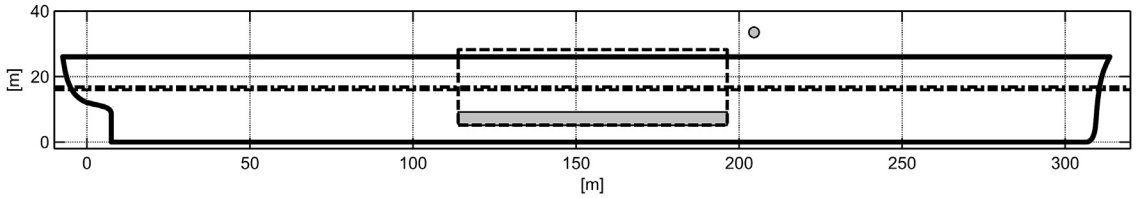

Fig. A.2. Side view of hull and tank geometry at ship centreplane. 200kDWT tanker. The point of heave measurement is also indicated.

Simulations have been performed by restraining the ship with two couples of springs positioned at the bow and at the stern of the vessel, respectively. The springs used in the simulations can provide a traction force (linear with respect to the spring elongation), but do not provide any force associated with compression. Such restrain layout qualitatively corresponds to the one outlined by de Kat (2000). In this way the vessel is softly restrained in sway, yaw and surge, with induced natural frequencies which are well below the range of wave frequencies used in the simulations. Similarly to the case of the Series 60 reported in the main text, also in this case a series of parameters were initially calculated or estimated, while a tuning process was carried out for a limited number of additional parameters by using only experimental data for the vessel without fluid in the tank. In particular, in this case, experimental data of roll motion in beam regular waves were used to tune the dry roll radius of gyration, as discussed before. Furthermore, an additional linear-in-velocity roll damping moment (in the form $-B_{L,add}\dot{\phi}$) and an additional quadratic-in-velocity roll damping moment ($-B_{Q,add}\dot{\phi}|\dot{\phi}|$) were used in order to tune the roll dissipation. An initial value for the additional linear roll damping coefficient $B_{L,add}$ was based on the analysis of the dimensionless roll damping coefficient from the experimental roll decay reported by de Kat (2000). Since the decay was carried out starting from a small initial amplitude of 5deg, the decay was not useful for the determination of nonlinear roll damping. The tuning of the additional quadratic damping coefficient $B_{Q,add}$ was therefore based on the available roll response in beam waves, and the same data were also used for further tuning of the additional linear damping coefficient $B_{L,add}$. After the tuning process the additional roll damping coefficients were fixed to $B_{L,add} = 7.0{\cdot}10^{8} N{\cdot}m/(rad/s)$ and $B_{Q,add} = 8.5{\cdot}10^{9} N{\cdot}m/(rad/s)^2$, with a centre of the ship-fixed reference system around which the moments are calculated positioned amidships, at the centreplane and on the waterplane in calm water. The drag coefficient for the cross flow model was originally fixed at a value of 0.8.

Simulations in regular beam waves have then been carried out in a range of frequencies corresponding to the range reported by de Kat (2000). In the description of the experimental tests, de Kat (2000) reports that "the wave height (crest-trough) was between 2 m and 3 m" and there was no reporting of the specific wave height for each tested wave frequency. For this reason, the wave height in the simulations carried out herein has been fixed to $H_w = 2.5m$ for all the frequencies. The number of particles used in the SPH solver was fixed to $1.0{\cdot}10^{4}$, i.e. to the same order of magnitude of that used for the Series 60. For the analysed wave conditions, the maximum speed induced by ship motions at the bottom of the tank in absence of fluid in the tank is about 1.2 m/s. This leads to a minimum limit for the speed of sound of 162 m/s according to (13), and this indicative limit is below the speed of sound of 200 m/s which has eventually been used in the present simulations. Simulations were run for a total time of 500s (full scale). Similarly to the case of the Series 60, also in this case the average amplitude of the motions (roll and heave) was measured considering the final part of each simulation (time window corresponding to final four full roll cycles or final 300s, whichever is minimum), and the motion amplitude is conventionally defined as half of the difference between maximum and minimum roll within each cycle.

Results from simulations with and without the tank are reported in Figure A3. To allow a comparison with the results reported by de Kat (2000), the amplitudes of roll (A_{roll}) and of heave (A_{heave}) have been normalised with respect to the wave amplitude $a_w = H_w/2$, which corresponds to 1.25 m in the simulations. It is however to be noted that normalisation with wave amplitude, although it is common and justifiable in the framework of linear ship motions, does not bring the same meaning of response amplitude operator when nonlinear motions are considered. Indeed, in case of nonlinear motions, the relation between the absolute forcing and the absolute response is, in general, nonlinear, and a linear response amplitude operator, therefore, does not exist. This comment is particularly relevant in case of roll motion, while it is less relevant in case of heave motion which behaves much more linearly with respect to the wave amplitude.

Results reported in Figure A3 show a very good agreement between experiments and simulations in case of empty tank, also thanks to the tuning process, and the agreement between experiments and simulations is good also for the case of partially filled tank. It can also be noticed that heave motion is very lightly influenced by the presence of the tank, with this small influence being more visible in the simulations than what can be noticed from the experimental data reported by de Kat (2000).

In this section the coupled numerical tool has therefore been successfully validated, with an overall satisfactory agreement between simulations and experiments with and without fluid in the tank, as reported in Figure A3.

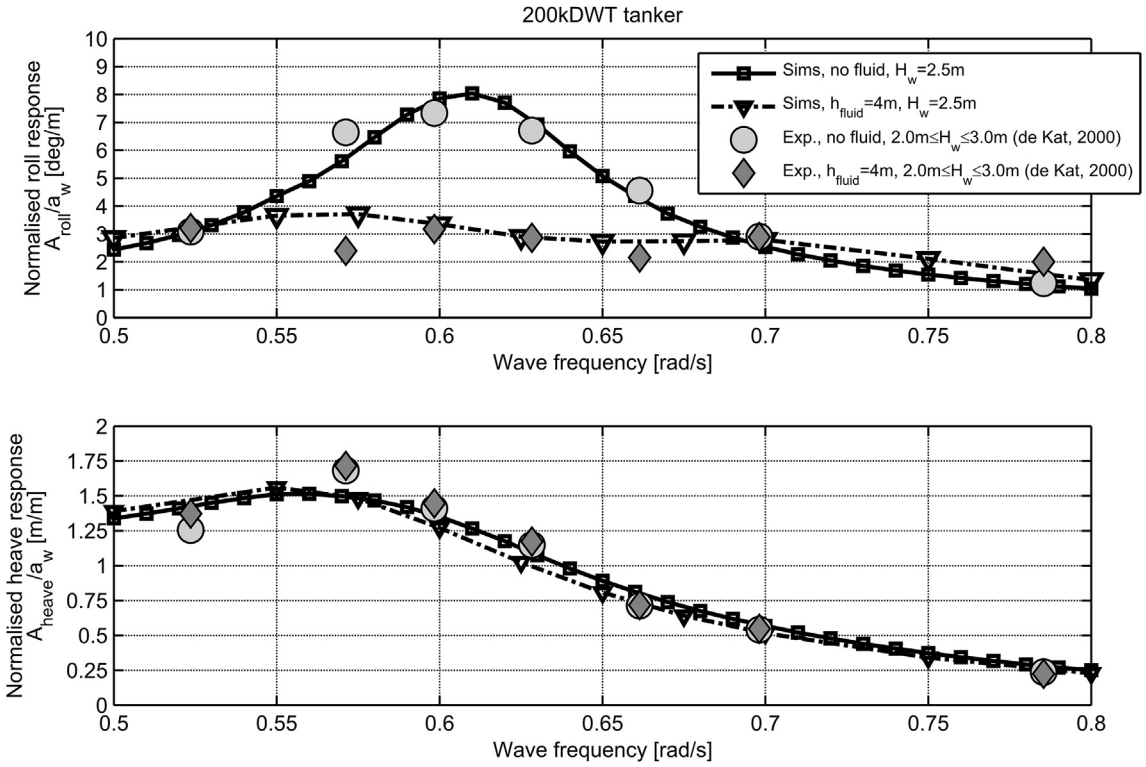

Fig. A.3. Roll and heave motions of the 200kDWT tanker. Comparison between simulations and experiments. Data reported at full scale.

References

Antuono, M., Colagrossi, A., Marrone, S., 2012. Numerical diffusive terms in weakly-compressible SPH schemes. Comput. Phys. Commun. 183, 2570–2580.

Antuono, M., Marrone, S., Colagrossi, A., Bouscasse, B., 2015. Energy balance in the δ-SPH scheme. Comput. Meth. Appl. Mech. Eng. 289, 209–226.

Artyszuk, J., 2006. A non-uniform current in ship manoeuvring. In: Proc. International Conference on Marine Simulation and Ship Manoeuvrability (MARSIM2006) (Terschelling, the Netherlands, June).

Bačkalov, I., Bulian, G., Cichowicz, J., Eliopoulou, E., Konovessis, D., Leguen, J.-F., Rosén, A., Themelis, N., 2016. Ship stability, dynamics and safety: Status and perspectives from a review of recent STAB and ISSW events. Ocean Eng. 116, 312–349. https://doi.org/10.1016/j.oceaneng.2016.02.016.

Bailey, P.A., Price, W.G., Temarel, P., 1998. A unified mathematical model describing the manoeuvring of a ship travelling in a seaway. Trans. RINA 140, 131–149.

Beck, R.F., Cummins, W.E., Dalzell, J.F., Mandel, P., Webster, W.C., 1989. Chapter 8-Motions in waves. In: Lewis, Edward V. (Ed.), Principles of Naval Architecture – Volume III – Motions in Waves and Controllability. The Society of Naval Architects and Marine Engineers.

Blume, P., 1979. Experimentelle Bestimmung von Koeffizienten der wirksamen Rolldämpfung und ihre Anwendung zur Abschätzung extremer Rollwinkel (in German), Schiffstechnik, Band 26, 3–23.

van den Bosch, J.J., Vugts, J.H., 1966. On roll damping by free-surface tanks. Trans. INA 69, 345–361.

Bouscasse, B., Antuono, M., Colagrossi, A., Lugni, C., 2013. Numerical and experimental investigation of nonlinear shallow water sloshing. Int. J. Nonlinear Sci. Numer. Simul. 14 (2), 123–138. https://doi.org/10.1515/ijnsns-2012-0100.

Bouscasse, B., Colagrossi, A., Souto-Iglesias, A., Cercos-Pita, J.L., 2014a. Mechanical energy dissipation induced by sloshing and wave breaking in a fully coupled angular motion system. I. Theoretical formulation and numerical investigation. Phys. Fluids (1994-present) 26 (3), 033103.

Bouscasse, B., Colagrossi, A., Souto-Iglesias, A., Cercos-Pita, J.L., 2014b. Mechanical energy dissipation induced by sloshing and wave breaking in a fully coupled angular motion system. II. experimental investigation. Phys. Fluids (1994-present) 26 (3), 033104.

Breuer, M., De Nayer, G., Münsch, M., Gallinger, T., Wüchner, R., 2012. Fluid–structure interaction using a partitioned semi-implicit predictor–corrector coupling scheme for the application of large-eddy simulation. J. Fluid Struct. 29, 107–130. https://doi.org/10.1016/j.jfluidstructs.2011.09.003.

Broglia, R., Bouscasse, B., Di Mascio, A., Lugni, C., Atsavapranee, P., 2009. Experimental and numerical analysis of the roll decay motion for a patrol boat. In: Proc. 19th International Offshore and Polar Engineering Conference (ISOPE2009), 21-26 June, pp. 709–716. Osaka, Japan.

Bulian, G., Francescutto, A., 2009. Experimental results and numerical simulations on strongly nonlinear rolling of multihulls in moderate beam seas. Proc. IME - Part M - J. Eng. Marit. Environ. 223, 189–210.

Bulian, G., Francescutto, A., 2011. Effect of roll modelling in beam waves under multi-frequency excitation. Ocean Eng. 38, 1448–1463.

Bulian, G., Francescutto, A., 2013. Second Generation Intact Stability Criteria: on the validation of codes for direct stability assessment in the framework of an example application. Pol. Marit. Res. 20, 52–61.

Bulian, G., Francescutto, A., Fucile, F., 2009. Determination of Relevant Parameters for the Alternative Assessment of Intact Stability Weather Criterion on Experimental Basis. University of Trieste. Final report HYD-III-CEH-5.

Bulian, G., Francescutto, A., Sinibaldi, M., 2012. Roll motion of a ship with low metacentric height in bi-chromatic beam waves. In: Proc. 11th International Conference on the Stability of Ships and Ocean Vehicles (STAB2012), 23-28 September, pp. 187–200. Athens, Greece.

Bulian, G., Moro, L., Brocco, E., Bresciani, F., Biot, M., Francescutto, A., September 2015. Using time domain nonlinear ship motion simulations to assess safety of people and cargo onboard a container vessel. In: Proc. 16th International Congress of the International Maritime Association of the Mediterranean (IMAM 2015) - Towards Green Marine Technology and Transport, pp. 99–110, 21-24 September, Pula, Croatia.

Bulian, G., Souto-Iglesias, A., Delorme, L., Botia-Vera, E., 2010. Smoothed particle hydrodynamics (SPH) simulation of a tuned liquid damper (TLD) with angular motion. J. Hydraul. Res. 48, 28–39. https://doi.org/10.3826/jhr.2010.0001. Extra Issue.

Bunnik, T., Veldman, A., 2010. Modelling the effect of sloshing on ship motions. In: Proc. 29th International Conference on Ocean, Offshore and Arctic Engineering (OMAE2010), 6–11 June. Shanghai, China, paper OMAE2010-20458.

Cardo, A., Francescutto, A., Nabergoj, R., 1981. Ultraharmonics and subharmonics in the rolling motion of a ship: steady-state solution. Int. Shipbuild. Prog. 28, 234–251.

Cardo, A., Francescutto, A., Nabergoj, R., 1982. On damping models in free and forced rolling motion. Ocean Eng. 9 (No. 2), 171–179.

Carette, N., 2015. A study of the response to sway motions of free surface anti-roll tanks. In: Proc. World Maritime Technology Conference 2015 (WMTC2015), 3–7 November. Providence, Rhode Island, USA, paper No. 133.

Carette, N.F.A.J., 2016. Fast time domain evaluation of Anti-Roll Tank and ship coupling using non-linear retardation functions. In: Proc. 15th International Ship Stability Workshop (ISSW2016), 13-15 June, pp. 59–66. Stockholm, Sweden.

Carrica, P.M., Sadat-Hosseini, H., Stern, F., 2012. CFD analysis of broaching for a model surface combatant with explicit simulation of moving rudders and rotating propellers. Comput. Fluids 53, 117–132.

Cercos-Pita, J.L., 2015. AQUAgpusph, a new free 3D SPH solver accelerated with OpenCL. Comput. Phys. Commun. 192, 295–312. https://doi.org/10.1016/j.cpc.2015.01.026.
Cercos-Pita, J.L., Souto-Iglesias, A., Gonzalez, L.M., Macià, F., 2013. AQUAgpusph, a free 3D SPH solver accelerated with OpenCL. In: Proc. 8th International SPHERIC Workshop, 4–6 June. Trondheim, Norway.
Cercos-Pita, J.L., Souto-Iglesias, A., Bulian, G., 2015. SHIXDOF-AQUAgpusph: nonlinear coupled ship motions and sloshing in free surface tanks. In: Proc. 10th SPHERIC International Workshop (SPHERIC2015), 16-18 June, pp. 288–295. Parma, Italy.
Cercos-Pita, J.L., Bulian, G., Pérez-Rojas, L., Francescutto, A., 2016. Coupled simulation of nonlinear ship motions and a free surface tank. Ocean Eng. 120, 281–288. https://doi.org/10.1016/j.oceaneng.2016.03.015.
Clarke, D., Gedling, P., Hine, G., 1983. The application of manoeuvring Criteria in hull design using linear theory. Trans. RINA 125, 45–68.
Colagrossi, A., Antuono, M., Touzé, D.L., 2009. Theoretical considerations on the free-surface role in the smoothed-particle-hydrodynamics model. Phys. Rev. 79 (5), 056701.
Colagrossi, A., Lugni, C., Landrini, M., 2001. Numerical and experimental transient tests for ship seakeeping. Int. J. Offshore Polar Eng. 11 (No. 3), 184–190.
Comer, D.E., 2013. Internetworking with TCP/IP – Vol. I: Principles, Protocols, and Architecture – Sixth Edition. Pearson (ISBN 978-0-13-608530-0).
Crespo, A.C., Dominguez, J.M., Barreiro, A., Gómez-Gesteira, M., Rogers, B.D., 2011. GPUs, a new tool of acceleration in CFD: efficiency and reliability on smoothed particle hydrodynamics methods. PLoS One 6, e20685. https://doi.org/10.1371/journal.pone.0020685.
Cummins, W.E., 1962. The impulse response function and ship motions. Schiffstechnik 47, 101–109.
de Kat, J.O., 2000. Dynamics of a ship with partially flooded compartment. In: Vassalos, D., Hamamoto, M., Papanikolaou, A., Molyneux, D. (Eds.), Contemporary Ideas on Ship Stability. Elsevier Science, pp. 249–263.
Dillingham, J., 1981. Motion studies of a vessel with water on deck. Mar. Technol. 18 (No. 1), 38–50.
Domínguez, J.M., Crespo, A.J.C., Gómez-Gesteira, M., 2013. Optimization strategies for CPU and GPU implementations of a smoothed particle hydrodynamics method. Comput. Phys. Commun. 184, 617–627.
Domínguez, J.M., Crespo, A.J.C., Barreiro, A., Rogers, B.D., Gómez-Gesteira, M., 2014. Efficient implementation of double precision in GPU computing to simulate realistic cases with high resolution. In: Proc. 9th SPHERIC International Workshop.
Elliott, A.S., Slattengren, J., Buijk, A., 2006. Fully Coupled Fluid/Mechanical Response Prediction for Truck-Mounted Tank Sloshing Using Cosimulation of MSC.ADAMS® and MSC.Dytran®. SAE Technical Paper No. 2006-01-0932. SAE International, Warrendale, PA.
Faltinsen, O., 1993. Sea Loads on Ships and Offshore Structures. Cambridge University Press.
Faltinsen, O.M., Timokha, A.N., 2009. Sloshing. Cambridge University Press.
Farhat, C., van der Zee, K.G., Geuzaine, P., 2006. Provably second-order time-accurate loosely-coupled solution algorithms for transient nonlinear computational aeroelasticity. Comput. Meth. Appl. Mech. Eng. Fluid-Struct. Interact. 195, 1973–2001. https://doi.org/10.1016/j.cma.2004.11.031.
Felippa, C.A., Park, K., Farhat, C., 2001. Partitioned analysis of coupled mechanical systems. Comput. Meth. Appl. Mech. Eng. 190, 3247–3270.
Ferrand, M., Laurence, D.R., Rogers, B.D., Violeau, D., Kassiotis, C., 2013. Unified semi-analytical wall boundary conditions for inviscid, laminar or turbulent flows in the meshless SPH method. Int. J. Numer. Meth. Fluid. 71, 446–472.
Field, S.B., Martin, J.P., 1976. Comparative effects of U-tube and free surface type passive roll stabilization systems. Trans. RINA 118, 73–92.
Fleissner, F., Lehnart, A., Eberhard, P., 2010. Dynamic simulation of sloshing fluid and granular cargo in transport vehicles. Veh. Syst. Dyn. 48, 3–15. https://doi.org/10.1080/00423110903042717.
Fonfach, J.M., Manderbacka, T., Neves, M.A.S., 2016. “Numerical sloshing simulations: comparison between Lagrangian and lumped mass models applied to two compartments with mass transfer”. Ocean Eng. 114, 168–184. https://doi.org/10.1016/j.oceaneng.2016.01.023.
Foster, I., Zhao, Y., Raicu, I., Lu, S., 2008. Cloud computing and grid computing 360-degree compared. In: IEEE Grid Computing Environments Workshop (GCE 2008), 12-16 November, pp. 1–10. https://doi.org/10.1109/GCE.2008.4738445. Austin, Texas, USA.
Francescutto, A., Contento, G., 1999a. An investigation on the applicability of simplified mathematical models to the roll-sloshing problem. Int. J. Offshore Polar Eng. 9 (2), 97–104. June.
Francescutto, A., Contento, G., 1999b. Bifurcations in ship rolling: experimental results and parameter identification technique. Ocean Eng. 26, 1095–1123.
Francescutto, A., Naito, S., 2004. Large amplitude rolling in a realistic sea. Int. Shipbuild. Prog. 51, 221–235.
Fujiwara, T., Haraguchi, T., 2005. Roll motion of Ro-Ro passenger ship with flooded vehicle deck. Int. J. Offshore Polar Eng. 15, 109–116.
Gao, Z., Gao, Q., Vassalos, D., 2013. Numerical study of damaged ship flooding in beam seas. Ocean Eng. 61, 77–87.
Göhner, U., 2010. Performance of implicit solver strategies on GPUs. In: Proc. 9th LS-DYNA Forum, Bamberg pp. N-I-1–6.
Gomes, J.P., Yigit, S., Lienhart, H., Schäfer, M., 2011. Experimental and numerical study on a laminar fluid–structure interaction reference test case. J. Fluid Struct. 27, 43–61. https://doi.org/10.1016/j.jfluidstructs.2010.09.004.
Graham, E.W., Rodriguez, A.M., 1952. The characteristics of fuel motion which affects airplane dynamics. J. Appl. Mech. 19, 381–388.
Greco, M., Lugni, C., 2012. 3-D seakeeping analysis with water on deck and slamming. Part 1: numerical solver. J. Fluid Struct. 33, 127–147.
Greco, M., Lugni, C., Faltinsen, O.M., 2014. Can the water on deck influence the parametric roll of a FPSO? A numerical and experimental investigation. Eur. J. Mech. B/Fluids 47, 188–201.
Hashimoto, H., Ito, Y., Kawakami, N., Sueyoshi, M., 2012. Numerical simulation method for coupling of tank fluid and ship roll motions. In: Proc. 11th International Conference on the Stability of Ships and Ocean Vehicles (STAB2012), 23-28 September, pp. 477–485. Athens, Greece.
Hayashi, C., 1964. Nonlinear Oscillations in Physical Systems. McGraw Hill, New York.
Hérault, A., Bilotta, G., Dalrymple, R.A., 2010. SPH on GPU with CUDA. J. Hydraul. Res. 48 (2010), 74–79. https://doi.org/10.1080/00221686.2010.9641247.
Himeno, Y., 1981. Prediction of Ship Roll Damping - A State of the Art. Technical Report No. 239. University of Michigan (September).
Holden, C., Fossen, T.I., 2012. A nonlinear 7-DOF model for U-tanks of arbitrary shape. Ocean Eng. 45, 22–37.
Huang, Z.-J., Hsiung, C.-C., 1996. Nonlinear shallow-water flow on deck coupled with ship motion. In: Proc. Twenty-first Symposium on Naval Hydrodynamics, 24-28 June, pp. 220–234. Trondheim, Norway.
Hughes, M.J., Kopp, P.J., Miller, R.W., 2011. Modelling of hull lift and cross flow drag forces in large waves in a computationally efficient dynamic stability prediction tool. In: Proc. 12th International Ship Stability Workshop (ISSW2011), 12-15 June, pp. 331–339. Washington D.C., USA.
IMO, 2009. International Code on Intact Stability, 2008-2009 Edition. International Maritime Organization, London, UK. ISBN 9280115065.
Jasionowski, A., 2001. An Integrated Approach to Damage Ship Survivability Assessment. Ph.D. thesis. University of Strathclyde.
Joosten, M.M., Dettmer, W.G., Perić, D., 2009. Analysis of the block Gauss–Seidel solution procedure for a strongly coupled model problem with reference to fluid–structure interaction. Int. J. Numer. Meth. Eng. 78, 757–778.
de Kat, J.O., Paulling, J.R., 1989. The simulation of ship motions and capsizing in severe seas. Trans. SNAME 97, 139–168.
Kawahara, Y., Maekawa, K., Ikeda, Y., 2009. A simple prediction formula of roll damping of conventional cargo ships on the basis of Ikeda's method and its limitations. In: Proc. 10th International Conference on the Stability of Ships and Ocean Vehicles (STAB2009), pp. 387–398. St. Petersburg, Russia, 22–26 June.
Kawamura, K., Hashimoto, H., Matsuda, A., Terada, D., 2015. SPH simulation of ship behaviour in severe water-shipping situations. In: Proc. 12th International Conference on the Stability of Ships and Ocean Vehicles (STAB2015), pp. 433–440. Glasgow, Scotland, UK, 14–19 June.
Kijima, K., 2003. Some studies on the prediction for ship manoeuvrability. In: Proc. International Conference on Marine Simulation and Ship Maneuverability (MARSIM2003) pp. KN-3-1 – KN-3-10.
Kim, B., Shin, Y.S., 2008. Coupled seakeeping with liquid sloshing in ship tanks. In: Proc. ASME 27th International Conference on Offshore Mechanics and Arctic Engineering (OMAE2008), 15-20 June, vol. 6, pp. 247–257.
Kim, Y., Nam, B.W., Kim, D.W., Kim, Y.S., 2007. Study on coupling effects of ship motion and sloshing. Ocean Eng. 34, 2176–2187.
Lee, B.S., Vassalos, D., 1996. An investigation into the stabilization effects of anti-roll tanks with flow obstructions. Int. Shipbuild. Prog. 43 (No. 433), 70–88.
Liut, D.A., Weems, K.M., Tin-Guen, Y., 2013. A quasi-three-dimensional finite-volume sallow water model for Green water on deck. J. Ship Res. 57, 125–140.
Macià, F., González, L.M., Cercos-Pita, J.L., Souto-Iglesias, A., 2012. A boundary integral SPH formulation. Consistency and applications to ISPH and WCSPH. Prog. Theor. Phys. 128, 439–462.
Malenica, Š., Zalar, M., Chen, X.B., 2003. Dynamic coupling of seakeeping and sloshing. In: Proc. 13th International Offshore and Polar Engineering Conference (ISOPE2003), 25-30 May, vol. III, pp. 486–492. Honolulu, Hawaii.
Manderbacka, T.L., Jacob, V., Carriot, T., Mikkola, T., Matusiak, J.E., 2014. Sloshing forces on a tank with two compartments, application of the pendulum model and CFD. In: Proc. of the ASME 2014 33rd International Conference on Ocean, Offshore and Arctic Engineering (OMAE 2014), 8–13 June. San Francisco, USA, OMAE2014-23355.
Manderbacka, T., Mikkola, T., Ruponen, P., Matusiak, J., 2015. Transient response of a ship to an abrupt flooding accounting for the momentum flux. J. Fluid Struct. 57, 108–126. https://doi.org/10.1016/j.jfluidstructs.2015.06.001.
Marrone, S., Colagrossi, A., Di Mascio, A., Le Touzé, D., 2015. Prediction of energy losses in water impacts using incompressible and weakly compressible models. J. Fluid Struct. 54, 802–822. https://doi.org/10.1016/j.jfluidstructs.2015.01.014.
Matusiak, J., 2007. On certain types of ship responses disclosed by the two-stage approach to ship dynamics. Arch. Civil Mech. Eng. 7, 151–166. https://doi.org/10.1016/S1644-9665(12)60233-7.
Mitra, S., Wang, C.Z., Hai, L.V., Reddy, J.N., Khoo, B.C., 2012. A 3D fully coupled analysis of nonlinear sloshing and ship motion. Ocean Eng. (39), 1–13 (and Corrigendum Ocean Eng. 52 (2012), 2012, 128).
el Moctar, O., Shigunov, V., Zorn, T., 2012. Duisburg test case: post-panamax container ship for benchmarking. Ship Technol. Res. 59, 50–64. https://doi.org/10.1179/str.2012.59.3.004.
Moirod, N., Baudin, E., Gazzola, T., Diebold, L., 2010. Experimental and numerical investigations of the global forces exerted by fluid motions on LNGC prismatic tanks boundaries. In: Proc. 20th International Offshore and Polar Engineering Conference (ISOPE2010), vol. III, pp. 10–17. Beijing, China, June 20-25.
Monaghan, J.J., 2005. Smoothed particle hydrodynamics. Rep. Prog. Phys. 68, 1703–1759.
Monaghan, J.J., 2012. Smoothed particle hydrodynamics and its diverse applications. Annu. Rev. Fluid Mech. 44, 323–346.
Neves, M.A.S., Merino, J.A., Rodríguez, C.A., 2009. A nonlinear model of parametric rolling stabilization by anti-roll tanks. Ocean Eng. 36, 1048–1059.

Oh, K.-G., Hasegawa, K., 2013. Low speed ship manoeuvrability: mathematical model and its simulation. In: Proc. of the ASME 2013 32nd International Conference on Ocean, Offshore and Arctic Engineering (OMAE 2013), 9–14 June. Nantes, France, OMAE2013-11489.

Papanikolaou, A., Spanos, D., 2004. 24th ITTC benchmark study on numerical prediction of damage ship stability in waves - Preliminary analysis of results. In: Proc. 7th International Ship Stability Workshop (ISSW2004), 1-3 November 1-3, pp. 1–9. Shanghai, China.

Papanikolaou, A., Zaraphonitis, G., Spanos, D., Boulougouris, E., Elipoulou, E., 2000. Investigation into the capsizing of damaged ro–ro passenger ships in waves. In: Proc. 7th International Conference on Stability of Ships and Ocean Vehicles (STAB2000), A, pp. 351–362. Launceston, Tasmania, Australia.

Peric, M., Zorn, T., el Moctar, O., Schellin, T.E., Kim, Y.-S., 2009. Simulation of sloshing in LNG-tanks. J. Offshore Mech. Arctic Eng. 131, 031101-1–031101-11. https://doi.org/10.1115/1.3058688.

Peters, W., Belenky, V., Bassler, C., Spyrou, K., Umeda, N., Bulian, G., Altmayer, B., 2011. The second generation intact stability Criteria: an overview of development. Trans. SNAME 119, 225–264.

Roberts, J.B., Spanos, P.D., 2003. Random Vibration and Statistical Linearization (Dover Publications).

Sadat-Hosseini, H., Carrica, P., Stern, F., Umeda, N., Hashimoto, H., Yamamura, S., Mastuda, A., 2011. CFD, system-based and EFD study of ship dynamic instability events: surf-riding, periodic motion, and broaching. Ocean Eng. 38, 88–110. https://doi.org/10.1016/j.oceaneng.2010.09.016.

Sadat-Hosseini, H., Stern, F., Olivieri, A., Campana, E.F., Hashimoto, H., Umeda, N., Bulian, G., Francescutto, A., 2010. Head-wave parametric rolling of a surface combatant. Ocean Eng. 37, 859–878.

Serván-Camas, B., Cercós-Pita, J.L., Colom-Cobb, J., García-Espinosa, J., Souto-Iglesias, A., 2016. Time domain simulation of coupled sloshing–seakeeping problems by SPH–FEM coupling. Ocean Eng. 123, 383–396. https://doi.org/10.1016/j.oceaneng.2016.07.003.

Sicklinger, S., Belsky, V., Engelmann, B., Elmqvist, H., Olsson, H., Wüchner, R., Bletzinger, K.-U., 2014. Interface jacobian-based co-simulation. Int. J. Numer. Meth. Eng. 98, 418–444. https://doi.org/10.1002/nme.4637.

Sinibaldi, M., Bulian, G., 2014. Towing simulation in wind through a nonlinear 4-DOF model: Bifurcation analysis and occurrence of fishtailing. Ocean Eng. 88, 366–392.

Souto-Iglesias, A., Macià, F., González, L.M., Cercos-Pita, J.L., 2013. On the consistency of MPS. Comput. Phys. Commun. 184, 732–745. https://doi.org/10.1016/j.cpc.2012.11.009.

Souto-Iglesias, A., Macià, F., González, L.M., Cercos-Pita, J.L., 2014. Addendum to “On the consistency of MPS [Comput. Phys. Commun. 184(3) (2013) 732–745]”. Comput. Phys. Commun. 185, 595–598. https://doi.org/10.1016/j.cpc.2013.10.018.

Spanos, D., Papanikolaou, A., 2001. On the stability of fishing vessels with trapped water on deck. Ship Technology Research—Schiffstechnik 48, 124–133.

Tanizawa, K., Taguchi, H., Sawada, H., 2003. Application of NWT to the design of ART. In: Proceedings of the Thirteenth International Offshore and Polar Engineering Conference (OMAE2003), 25-30 May, pp. 307–314. Honolulu, Hawaii, USA.

Taguchi, H., Sawada, H., Tanizawa, K., 2003. A study on complicated roll motion of a ship equipped with an anti-rolling tank. In: Proc. 8th International Conference on Stability of Ships and Ocean Vechicles (STAB2003), 15-19 September, pp. 607–616. Madrid, Spain.

Todd, F.H., Stuntz, G.R., Pien, P.C., 1957. Series 60-the effect upon resistance and power of variation in ship proportions. Trans. SNAME 65, 445–589.

Toxopeus, S.L., 2006. Validation of slender-body method for prediction of linear manoeuvring coefficients using experiments and viscous-flow calculations. In: Proc. 7th International Conference on Hydrodynamics (ICHD2006), pp. 493–502. Ischia.

Tzamtzis, S., 2004. Development and Testing of a Procedure for the Alternative Assessment of Weather Criterion on Experimental Basis. University of Trieste and National Technical University of Athens.

Wheeler, J.D., 1969. Method for calculating forces produced by irregular waves. In: Offshore Technology Conference. Dallas, Texas, US, Paper No. 1006.

Zhao, W., Yang, J., Hu, Z., Tao, L., 2014. Coupled analysis of nonlinear sloshing and ship motions. Appl. Ocean Res. 47, 85–97.